



Research paper

Responses of the terrestrial carbon cycle to drought over China: Modeling sensitivities of the interactive nitrogen and dynamic vegetation

Binghao Jia ^{a,b,*}, Yuanyuan Wang ^c, Zhenghui Xie ^a^a State Key Laboratory of Numerical Modeling for Atmospheric Sciences and Geophysical Fluid Dynamics, Institute of Atmospheric Physics, Chinese Academy of Sciences, Beijing, China^b Plateau Atmosphere and Environment Key Laboratory of Sichuan Province, Chengdu, China^c Beijing Meteorological Observatory, Beijing, China

ARTICLE INFO

Article history:

Received 30 April 2017

Received in revised form 9 November 2017

Accepted 11 November 2017

Keywords:

Drought

Terrestrial carbon cycle

CLM4.5

Interactive nitrogen cycle

Dynamic vegetation

Standardized precipitation index

ABSTRACT

Drought can trigger both immediate and time-lagged responses of terrestrial ecosystems and even cause sizeable positive feedbacks to climate warming. In this study, the influences of interactive nitrogen (N) and dynamic vegetation (DV) on the response of the carbon cycle in terrestrial ecosystems of China to drought were investigated using the Community Land Model version 4.5 (CLM4.5). Model simulations from three configurations of CLM4.5 (C, carbon cycle only; CN, dynamic carbon and nitrogen cycle; CNDV, dynamic carbon and nitrogen cycle as well as dynamic vegetation) between 1961 and 2010 showed that the incorporation of a prognostic N cycle and DV into CLM4.5 reduce the predicted annual means and inter-annual variability of predicted gross primary production (GPP) and net ecosystem production (NEP), except for a slight increase in NEP for CNDV compared to CN. They also resulted in better agreement with the gridded flux data upscaled from eddy covariance observations (7.0 PgC yr^{-1}) of annual GPP over the terrestrial ecosystems in China for CLM45-CN (7.5 PgC yr^{-1}) and CLM45-CNDV (7.3 PgC yr^{-1}) than for CLM45-C (10.9 PgC yr^{-1}). Compared to the CLM45-C, the carbon-nitrogen coupling strengthened the predicted response of GPP to drought, resulting in a higher correlation with the standardized precipitation index (SPI; $r_C = 0.62$, $r_{CN} = 0.67$), but led to a weaker sensitivity of NEP to SPI ($r_C = 0.51$, $r_{CN} = 0.45$). The CLM45-CNDV had the longest lagged responses of GPP to drought among the three configurations.

© 2017 Elsevier B.V. All rights reserved.

1. Introduction

As a major sink in the global carbon cycle, terrestrial ecosystems have sequestered 25%–30% of anthropogenic carbon dioxide (CO_2) emissions for the past five decades (Le Quéré et al., 2009). Terrestrial ecosystems slow increases in atmospheric CO_2 concentration by sequestering carbon in the vegetation biomass and soils, providing a negative feedback mechanism in the climate–carbon system (Chen et al., 2011; Pan et al., 2011; Reichstein et al., 2013; Zhao and Running, 2010). The occurrence of extreme climatic events (e.g., drought) can affect the functioning of the carbon cycle in terrestrial ecosystems by reducing photosynthetic capacity or altering respiratory processes (Zeng et al., 2005; Zscheischler et al., 2014). Severe regional drought has become more frequent under a chang-

ing climate and is likely to increase in frequency for the foreseeable future (Dai, 2013; Qian et al., 2011; Stocker et al., 2013). China experienced frequent severe droughts during the second half of the 20th century (Zou et al., 2005) and faces a projected increase in drought risk in the future (Wang and Chen, 2014). Therefore, it is necessary to explore the impact of drought on the carbon fluxes of terrestrial ecosystems; this will advance our understanding of the mechanism of carbon and water coupling under drought conditions and provide information needed for policy-making.

Site-level measurements from a global observation network (Schwalm et al., 2010; Sun et al., 2006) and satellite-based observations (Zhang et al., 2012; Zhao and Running, 2010; Zscheischler et al., 2014) usually have been used to quantify the impacts of drought on the carbon fluxes of terrestrial ecosystems. Compared to in situ and satellite-based observations, process-based terrestrial carbon cycle models can better capture the coupling mechanism between increasing climate extremes and decreasing carbon uptake (Reichstein et al., 2013; Zeng et al., 2005) and have been used to examine the response of the terrestrial carbon cycle to droughts over China (Liu et al., 2014; Pei et al., 2013; Xiao et al., 2009; Yuan

* Corresponding author at: State Key Laboratory of Numerical Modeling for Atmospheric Sciences and Geophysical Fluid Dynamics, Institute of Atmospheric Physics, Chinese Academy of Sciences, Beijing, China.

E-mail address: bhjia@mail.iap.ac.cn (B. Jia).

et al., 2014). For example, Xiao et al. (2009) used a process-based biogeochemistry model, the Terrestrial Ecosystem Model, to investigate the impact of twentieth-century droughts on the terrestrial carbon cycle in China and found that severe and extended drought substantially reduced the countryside annual net primary production (NPP) and net ecosystem production (NEP). Moreover, results showed that strong decreases in NPP were mainly responsible for the anomalies in annual NEP during the drought periods; heterotrophic respiration also experienced a strong decrease, but with smaller magnitude (Xiao et al., 2009). Yuan et al. (2014) pointed that the multiyear precipitation reduction changed the regional carbon uptake of $0.011 \text{ PgC yr}^{-1}$ in Northern China from 1982 to 1998 to a net source of $0.018 \text{ PgC yr}^{-1}$ from 1999 to 2011, and the average maize yield from 1999 to 2011 was reduced by $440 \text{ kg ha}^{-1} \text{ yr}^{-1}$ compared with linear trend yields. During the summer of 2013, southern China experienced the strongest drought on record for the past 113 years, which significantly reduced the satellite-based vegetation index, GPP, and evapotranspiration (Xie et al., 2016) and altered the regional carbon cycle (Yuan et al., 2016).

As one of the most important factors in terrestrial carbon cycle, nitrogen (N) plays an important role in the coupling between carbon and water by affecting photosynthetic rates and stomatal conductance (Bonan and Levis, 2010; Gotangco Castillo et al., 2012; Thornton et al., 2009). The process of carbon–nitrogen–water coupling leads to a change in canopy transpiration; the changing transpiration then affects photosynthesis through water stress (Lee et al., 2013). Furthermore, N limitation can decrease the positive effect of CO_2 fertilization on the vegetation productivity in unmanaged ecosystems (Langley and Megonigal, 2010); leaf photosynthesis may be more sensitive to reduced stomatal conductance at elevated CO_2 levels when N is limited (McMurtrie et al., 2008). In addition, dynamic vegetation (DV) models have been designed to be coupled with some land surface models for the study of global ecosystem–climate interactions (Zeng et al., 2008). The incorporation of DV in land models has been found to reduce the seasonal variability in predicted leaf area and moisture fluxes (Gotangco Castillo et al., 2012) and enhance climate persistence in earth system models by introducing long-term memory to the earth system (Delire et al., 2004). However, few studies have examined the influences of including the N cycle and DV on simulating the responses of terrestrial carbon cycle to drought.

The process-based model, Community Land Model version 4.5 (CLM4.5) (Oleson et al., 2013) has an option for running a prognostic carbon–nitrogen model (Thornton et al., 2007) or a dynamic global vegetation model (Gotangco Castillo et al., 2012; Levis et al., 2004; Zeng et al., 2008) or both. In this study, it was used to present an analysis on the relationships between drought (indicated by the standardized precipitation index, SPI) and vegetation production in China. The model simulations were compared with gridded observational carbon flux data (Jung et al., 2009, 2011). The objectives of this study were to (1) explore the diverse impacts of the interactive N and DV on the simulated changes in the response of terrestrial ecosystem carbon cycle to drought, (2) investigate such responses across plant functional types and climatic regions, and (3) discuss why the carbon–nitrogen coupling and dynamical vegetation would predict different responses to drought compared to the carbon-only configuration.

2. Model and methods

2.1. Model descriptions

The CLM4.5 model is the latest version of the CLM family and contains detailed biophysics, hydrology, and biogeochemistry representations (Oleson et al., 2013). Compared to previous versions,

CLM4.5 has many new modifications in the physical and biogeochemical parameterizations (Bonan et al., 2011; Koven et al., 2013; Li et al., 2013; Oleson et al., 2013).

The CLM4.5 model can be operated with a dynamic carbon cycle only (CLM45-C) or with an interactive carbon–nitrogen cycle (CLM45-CN). In addition, the CLM45-CN model configuration includes an option to include vegetation dynamics (CLM45-CNDV). A general description of the carbon–nitrogen cycle and dynamic vegetation processes in CLM4.5 is provided in Section 2.1.1 and 2.1.2, respectively. Further detailed descriptions can be found in Oleson et al. (2013).

2.1.1. Carbon–nitrogen cycle

In the CLM45-CN model the biophysical framework of CLM (Oleson et al., 2013) is merged with the prognostic carbon and nitrogen dynamics of the terrestrial biogeochemistry model Biome-BGC (Biome BioGeochemical Cycles) (Thornton and Rosenbloom, 2005). The integrated model is fully prognostic with respect to all carbon and nitrogen state variables in the vegetation, litter, and soil organic matter, and retains all prognostic quantities for water and energy in the vegetation snow-soil column from CLM4.5. These state variables are tracked for leaf, live stem, dead stem, live coarse root, dead coarse root, and fine root pools.

In CLM45-CN, the maximum rate of carboxylation (V_{cmax}) for leaf-level photosynthesis is calculated as following (Thornton and Zimmermann, 2007):

$$V_{cmax} = V_{cmax25} \cdot f(T_v) \cdot f(DYL) \cdot \beta_t, \quad (1)$$

$$V_{cmax25} = N_a \cdot F_{LNR} \cdot F_{NR} \cdot a_{R25}, \quad (2)$$

where V_{cmax25} is the maximum rate of carboxylation at 25°C ; T_v and DYL are leaf temperature and day-length, respectively; N_a is the area-based N concentration, F_{LNR} , F_{NR} , and a_{R25} are three constant parameters, which represent the fraction of leaf N in Rubisco, the mass ratio of total Rubisco molecular mass to N in Rubisco, and the specific activity of Rubisco, respectively. β_t is a soil water stress function, representing the influences of soil moisture on leaf-level photosynthesis. In addition, soil water has a direct effect on the leaf stomatal conductance g_s (i.e., the inverse of stomatal resistance r_s) through the Ball–Berry conductance model expressed as Eq. (3) (Collatz et al., 1991):

$$\frac{1}{r_s} = g_s = m \frac{A_n}{c_s/P_{atm}} h_s + b \beta_t, \quad (3)$$

where m is a plant functional type (PFT) dependent parameter, A_n is leaf net photosynthesis, c_s is the CO_2 partial pressure at the leaf surface, P_{atm} is the atmospheric pressure, h_s is the leaf surface humidity, b is the minimum stomatal conductance, and β_t is a soil water stress function. The function β_t ranges from one when the soil is wet to near zero when the soil is dry and is given:

$$\beta_t = \sum_i w_i r_i, \quad (4)$$

where w_i is a plant wilting factor and depends on the soil water potential of each soil layer; r_i is the distribution of roots in layer i and depends on the plant functional type (Oleson et al., 2013). Eq. (4) suggests that soil moisture estimations affect the accuracy of terrestrial carbon fluxes through the soil water stress function β_t ; in turn, β_t has a large impact on soil water content simulation through the transpiration in each layer, called the “soil moisture sink term” (evapotranspiration loss) in the soil water equation (Jia et al., 2013a).

The canopy-level photosynthesis (or gross primary production, GPP) is derived by summing the sunlit and shaded leaf-level photosynthesis rates multiplied by the sunlit and shaded leaf area indices, including potential reductions due to limited availability of mineral

nitrogen (Oleson et al., 2013). The carbon available for allocation to new growth is calculated at each model time step. Total plant nitrogen demand for each time step is calculated from the carbon allometry and nitrogen concentration for each tissue type specified by the PFT. Overall, the leaf-level photosynthesis is used to calculate the GPP, and GPP is scaled by the nitrogen limitation factor in the carbon and nitrogen allocation module.

The CLM45-CN model also simulates both autotrophic (R_a) and heterotrophic respiration (R_h). Autotrophic respiration is equivalent to the sum of maintenance respiration (R_m) and growth respiration (R_g): R_m is calculated as a function of the temperature and N concentration of live tissues (Thornton and Rosenbloom, 2005) and R_g is calculated as a constant fraction (0.3) of the carbon allocated to growth. Heterotrophic respiration is the carbon released to the atmosphere during the decomposition of litter and soil organic matter.

The NPP is calculated by removing the autotrophic respiration R_a from the GPP (Eq. (5)):

$$NPP = GPP - R_a, \quad (5)$$

and the NEP is the balance between NPP and R_h (Eq. (6)):

$$NEP = NPP - R_h = GPP - R_e, \quad (6)$$

where ecosystem respiration (R_e) is the sum of the R_a and R_h . Positive values of NEP indicate net carbon gain by the ecosystem (i.e., the ecosystem is a carbon sink) and negative values signify a net carbon loss (i.e., the ecosystem is a carbon source).

2.1.2. Dynamic vegetation

The CLM45-CNDV model can simulate only unmanaged vegetation, which includes the tree, grass, and shrub PFTs, using biogeography rules that are climate-based (Gotangco Castillo et al., 2012; Oleson et al., 2013). Crops may exist in the carbon–nitrogen component, but the interactive crop management model was not included in the simulations performed for the present study.

In CLM45-CNDV, tree mortality occurs as a result of fire, anthropogenic land cover change, wind throw, insect attack, disease, heat stress, low growth efficiency, and increasing age (Levis et al., 2004; Oleson et al., 2013). The latter two effects are directly or indirectly driven by climatic trends and correspond best to the type of mortality events that have been reported for the field sites. Drought reduces the growth efficiency of trees (expressed as NPP per leaf area); when a PFT ends the year with negative NPP, it is removed from the grid cell and its carbon is converted to litter. The age-related mortality can be influenced indirectly by drought episodes since water scarcity changes the composition of trees in terms of their maximum non-stressed longevity (Levis et al., 2004).

2.1.3. Atmospheric forcing data

In this study, CLM4.5 was forced using a 110 year (1901–2010) observation-based atmospheric forcing data set, the Climate Research Unit (CRU)–National Centers for Environmental Prediction (NCEP) reanalysis (CRUNCEP) (Viovy, 2011); this data set comprises six hourly interval data on precipitation, solar radiation, air temperature, pressure, humidity and wind. It is a combination of two existing datasets: the CRU TS3.2 half-degree monthly data, covering the period 1901–2002 (Mitchell and Jones, 2005), and the NCEP reanalysis 2.5°, six hourly data, covering the period from 1948 to near present. The CRUNCEP dataset has been used to force the CLM in several studies of vegetation growth, evapotranspiration, and the terrestrial carbon cycle (Mao et al., 2012; Piao et al., 2012; Shi et al., 2013).

2.2. Experimental design

In this study, the control experiment was a default CLM45-C simulation with prescribed nitrogen limitation (Bonan and Lewis, 2010; Thornton et al., 2007). The “treatments” were the CLM45-CN and CLM45-CNDV simulations, which used the same atmospheric forcing data as the CLM45-C simulation, but the spin-up processes were slightly different. Based on the sub-data set from 1901 to 1960, the CLM45-C and CLM45-CN simulations were first spun-up using land cover, atmospheric CO₂, and N deposition levels from the year 1850 to attain a near-equilibrium state. Then, they were run to 1961, forced by repeating the 60 year sub-data set (1901–1960) with the transient CO₂ concentration, N deposition and historical land use data spanning 1850–1960, to obtain the initial conditions for the start of simulations.

A complete spin-up of the DV in CLM4.5 first requires establishment of the carbon and nitrogen pools and fluxes. In this study, the process for spinning up CLM45-CNDV was similar to that of Gotangco Castillo et al. (2012); beginning from the end of the CLM45-CN transient simulation in 1850, the DV was spun up from bare ground in a 2400-year offline CLM45-CNDV simulation, with repeating 1901–1960 meteorological variables, performed as an equilibrium spin-up. After that, the 60-year data were used to force the CLM45-CNDV and obtain the initial conditions for the year 1961.

Finally, the 1961–2010 atmospheric forcing data were used to force the three simulations (CLM45-C, CLM45-CN, and CLM45-CNDV) using initial conditions from 1961. CLM45-C and CLM45-CN used the surface data for the year 2000 while CLM45-CNDV updates biogeography annually (Gotangco Castillo et al., 2012; Oleson et al., 2013). Noted that all simulations were performed at a horizontal resolution of 0.5° × 0.5° and in half-hour time steps and the CO₂ concentration was held fixed at year 2000 levels, 368.9 ppmv (Gotangco Castillo et al., 2012). In this study, the focus was on comparing the three simulations over the past five decades (1961–2010). Some results are considered within specific sub-regions in China, defined as such according to regional climatic characteristics (Fig. 1a) (Liu et al., 2014; Pei et al., 2013; Piao et al., 2009).

2.3. Observational data for evaluation

Jung et al. (2011) generated a gridded carbon flux data set by upscaling FLUXNET measurements from eddy covariance flux tower sites to the global scale using the machine learning technique, model tree ensembles (hereafter MTE, Jung et al., 2009). The MTEs were first trained to predict carbon fluxes at site-level based on remote sensing indices, climate and meteorological data, and information on land use. Then, the trained MTEs were applied to generate global fields at a 0.5° × 0.5° spatial resolution with a monthly temporal resolution (Jung et al., 2011). The MTE data used in this study include GPP and net ecosystem exchange (NEE) covering the mainland China from 1982 to 2010. Although the MTE data are not direct carbon flux measurements, they have been proved to agree better with the FLUXNET observations than some ecosystem models (Jung et al., 2011; Wang et al., 2015). For example, modeling efficiency and root mean square error (RMSE) of mean GPP at the site level is 0.74 and 270 gC m⁻² yr⁻¹ while the RMSE of three ecosystem models (LPJ, Orchidee, Biome-BGC) for the GPP of forests in Europe was about 420 gC m⁻² yr⁻¹. Wang et al. (2015) found that, compared to the CLM4-CN, the MTE data agreed better with ground-based GPP observations with lower RMSEs (38 and 11 gC m⁻² month⁻¹ for the forest and grass, respectively) and higher correlation coefficients (0.9 and 0.99 for the forest and grass, respectively). In addition, the CO₂ fertilization effect is not explicitly included in this dataset, the same configuration as the simulations

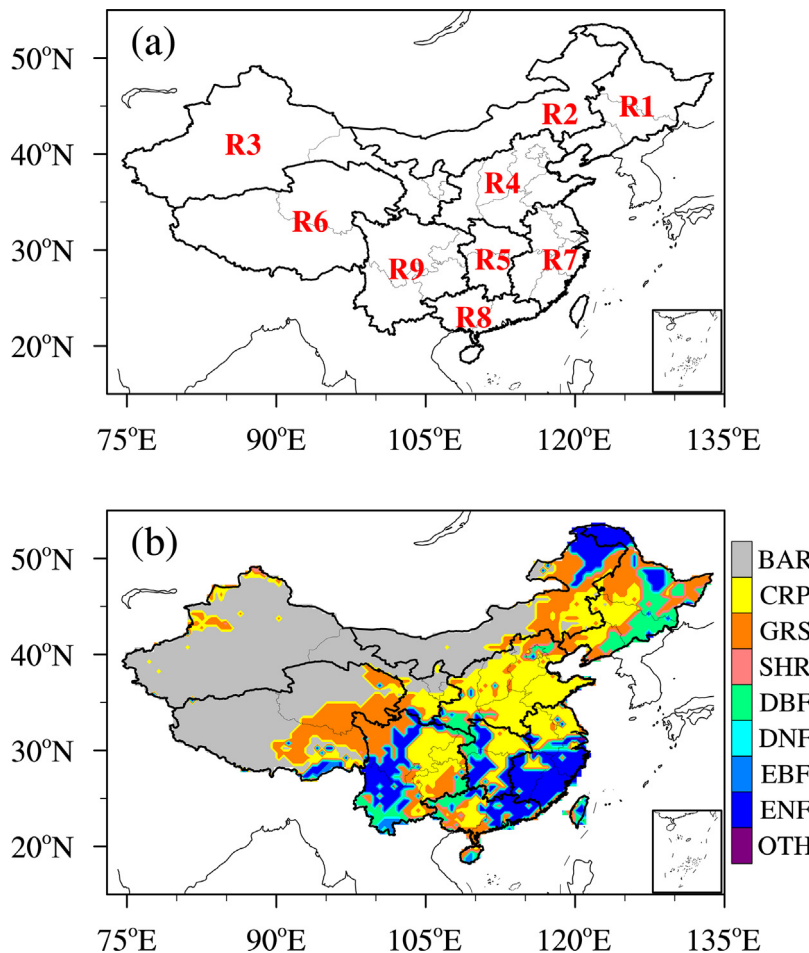


Fig. 1. The spatial distributions of (a) nine sub-regions (R1–R9) in China; and (b) plant functional types (PFT). R1: northeast China (Heilongjiang, Jilin, Liaoning); R2: Inner Mongolia; R3: northwest China (Gansu, Ningxia, Xinjiang); R4: north China (Beijing, Hebei, Henan, Shandong, Shanxi, Shaanxi, Tianjin); R5: central China (Hubei, Hunan); R6: Tibetan Plateau (Qinghai, Tibet); R7: southeast China (Anhui, Fujian, Jiangsu, Jiangxi, Shanghai, Taiwan, Zhejiang); R8: south China (Guangdong, Guangxi, Hainan, Hongkong, Macao); and R9: southwest China (Guizhou, Sichuan, Yunnan, Chongqing). The PFT information is shown in Table 2.

of this work. Therefore, we used the MTE data as the “reference” to evaluate the three CLM4.5 simulations in the present study.

2.4. Methods

Researchers have developed many indexes to monitor different types of drought (McKee et al., 1993; Palmer, 1965; Vicente-Serrano et al., 2010). As one of the simplest drought indexes, SPI has been proved to be suitable for quantifying most drought events (Lloyd Hughes and Saunders, 2002). Furthermore, the SPI commonly has been used to consider the effect of drought on the terrestrial carbon cycle due to its simplicity, temporal flexibility and spatial consistency (Liu et al., 2014; Pei et al., 2013). Since only the effect of precipitation was considered in this study, the SPI index was chosen as an appropriate index by which to quantify the drought severity in China. The SPI was computed by first fitting a probability density function (PDF) to the frequency distribution of precipitation over a specific time scale of interest. This was performed separately for each month (or whatever the temporal basis was of the raw precipitation time series) and for each spatial location. Each PDF was then transformed into a standardized normal distribution, with a mean of zero and a variance of one (Lloyd Hughes and Saunders, 2002; McKee et al., 1993). A clear and detailed description for calculating the SPI can be found in Lloyd Hughes and Saunders (2002). In the present study, the SPI with five running time intervals, i.e. 1, 3, 6, 9, 12 months, covering the period from 1961 to 2010, was used. Using

Table 1
Classifications of drought based on standardized precipitation index (SPI) values.

SPI values	Drought	Abbr.
$\text{SPI} \geq 2.0$	Extreme Wet	ExWe
$1.5 \leq \text{SPI} < 2.0$	Severe Wet	SeWe
$1.0 \leq \text{SPI} < 1.5$	Moderate Wet	MoWe
$0.5 \leq \text{SPI} < 1.0$	Mild Wet	MiWe
$-0.5 < \text{SPI} < 0.5$	Normal	Normal
$-1.5 < \text{SPI} \leq -0.5$	Mild Drought	MiDr
$-1.5 < \text{SPI} \leq -1.0$	Moderate Drought	MoDr
$-2.0 < \text{SPI} \leq -1.5$	Severe Drought	SeDr
$\text{SPI} \leq -2.0$	Extreme Drought	ExDr

Drought classification based on standardized precipitation index (SPI) values.

SPI as an indicator, a drought was considered to occur when the SPI was less than zero (McKee et al., 1993). As described by McKee et al. (1993) and Zhang et al. (2012), drought in a given year can be classified into nine categories, according to the 12-month SPI, through to the end of December (Table 1).

The effects of the drought on carbon flux are assessed using a standardized anomaly index (SAI) (Katz and Glantz, 1986), which has been used in past research (Liu et al., 2014; Lotsch et al., 2005; Pei et al., 2013). The SAI is defined as the standardized departure from the average values using Eq. (7):

$$\text{SAI}_i = \frac{CF_i - \text{Mean}}{\text{Std}}, \quad (7)$$

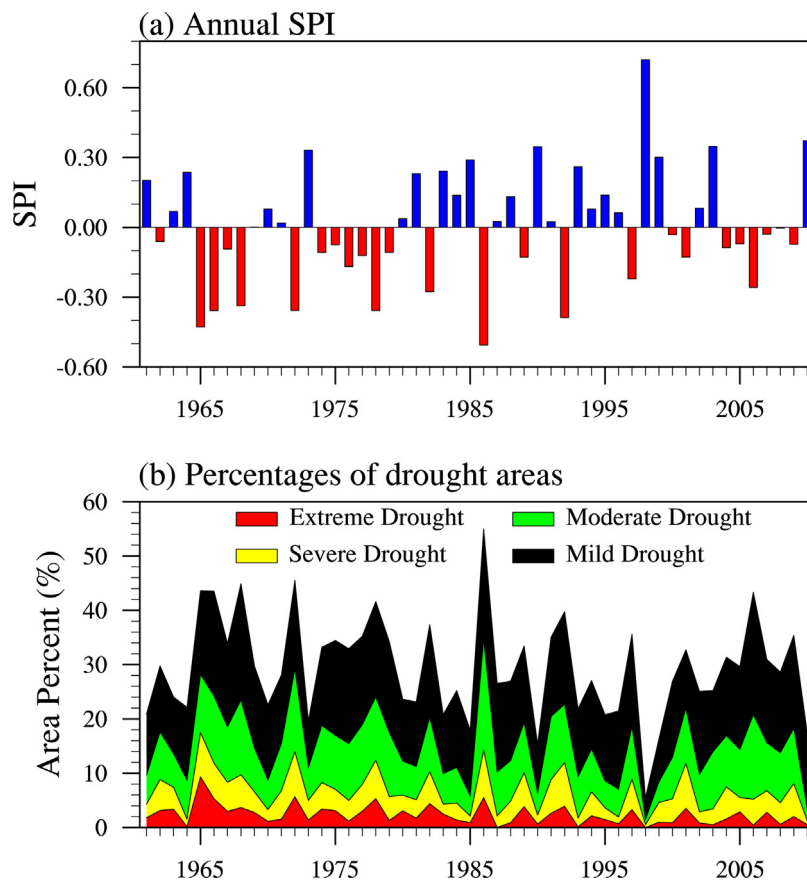


Fig. 2. Drought in China: (a) mean annual standardized precipitation index (SPI) across China; and (b) percentage of areas within China subjected to each severity of drought (see Table 1) from 1961 to 2010.

where CF_i is the carbon flux value for the year i ; and, Mean and Std are the mean and standard deviation, respectively, of the annual values from 1961 to 2010.

3. Results

3.1. Characterization of drought events in China during the past 50 years

During the past five decades (1961–2010), China witnessed several drought events, with different intensities and areal extents (Dai, 2013; Qian et al., 2011). The means of the annual SPI (the 12-month SPI through to the end of December), and the percentages of the total areas in China affected by different drought intensities in each year, show several years of extreme drought (Fig. 2). In particular, China experienced extensive drought in 1965, 1966, 1968, 1972, 1978 and 1986 between 1961 and 1990 ($SPI < -0.35$; Fig. 2a) when more than 24% of the total area in China was affected by moderate, severe, and extreme drought (Fig. 2b). The year 1986 showed the lowest value of spatially averaged SPI during the last 50 years ($SPI = -0.51$) and the area of China affected by severe and extreme drought was 15% (approximately 1.4 million km²); drought was also observed across approximately 750 ground-based meteorological stations (Liu et al., 2014). Over the last two decades (1991–2010), the drought events in 1997 and 2006 were the most serious ($SPI < -0.2$), as more than 20% of the area in China was affected by moderate, or even more severe drought.

According to the spatial distribution (Fig. 3) of drought during the key years identified above, most regions of China in 1986 experienced drought events, except for parts of southwest China, northeast China and northwest China (Fig. 3f). In 1972, vast areas of

China (14%) also experienced severe and extreme drought (Fig. 3d). Even though drought did not occur widely throughout China in 1965, the severity was mostly severe to extreme where drought occurred (18% of the total area of China), mainly in the Tibetan Plateau, Inner Mongolia and north China (Fig. 3a). Drought continued into 1966, but occurred in different areas, mainly the middle and southeastern areas of China. Southeast China and north China experienced severe drought in 1978 (Fig. 3e) and 1997 (Fig. 3g), whereas the drought events in 2006 were mostly mild (Fig. 3h).

3.2. Temporal variations of carbon fluxes and their responses to droughts

In general, the CLM45-C and CLM45-CN simulations exhibited a similar temporal variation in their carbon flux anomalies and showed a clear decline of terrestrial ecosystem productivity during periods of drought (Figs. S1a and S1b) due to the low soil water stress function β_t (Fig. S1d). Moreover, it is clearly seen from Fig. 4 that the carbon fluxes existed a significant decrease with the increase of drought intensity (the decrease of SPI). However, the introduction of the N cycle decreased the mean annual predicted carbon fluxes. For example, the annual GPP and NEP for the CLM45-CN simulation were 7.5 PgCyr^{-1} and 0.18 PgCyr^{-1} , respectively, compared to 10.9 PgCyr^{-1} and 0.53 PgCyr^{-1} , respectively, for the CLM45-C simulation. Furthermore, the CLM45-CN simulation predicted lower inter-annual variability (IAV) in GPP and NEP, as measured by the standard deviation, compared with the CLM45-C simulation. The IAVs of GPP and NEP for the CLM45-CN simulation were 0.27 PgCyr^{-1} and 0.21 PgCyr^{-1} , respectively, while $\text{Std}_{\text{GPP}} = 0.32 \text{ PgCyr}^{-1}$ and $\text{Std}_{\text{NEP}} = 0.26 \text{ PgCyr}^{-1}$ for the CLM45-C simulation (Fig. S1).

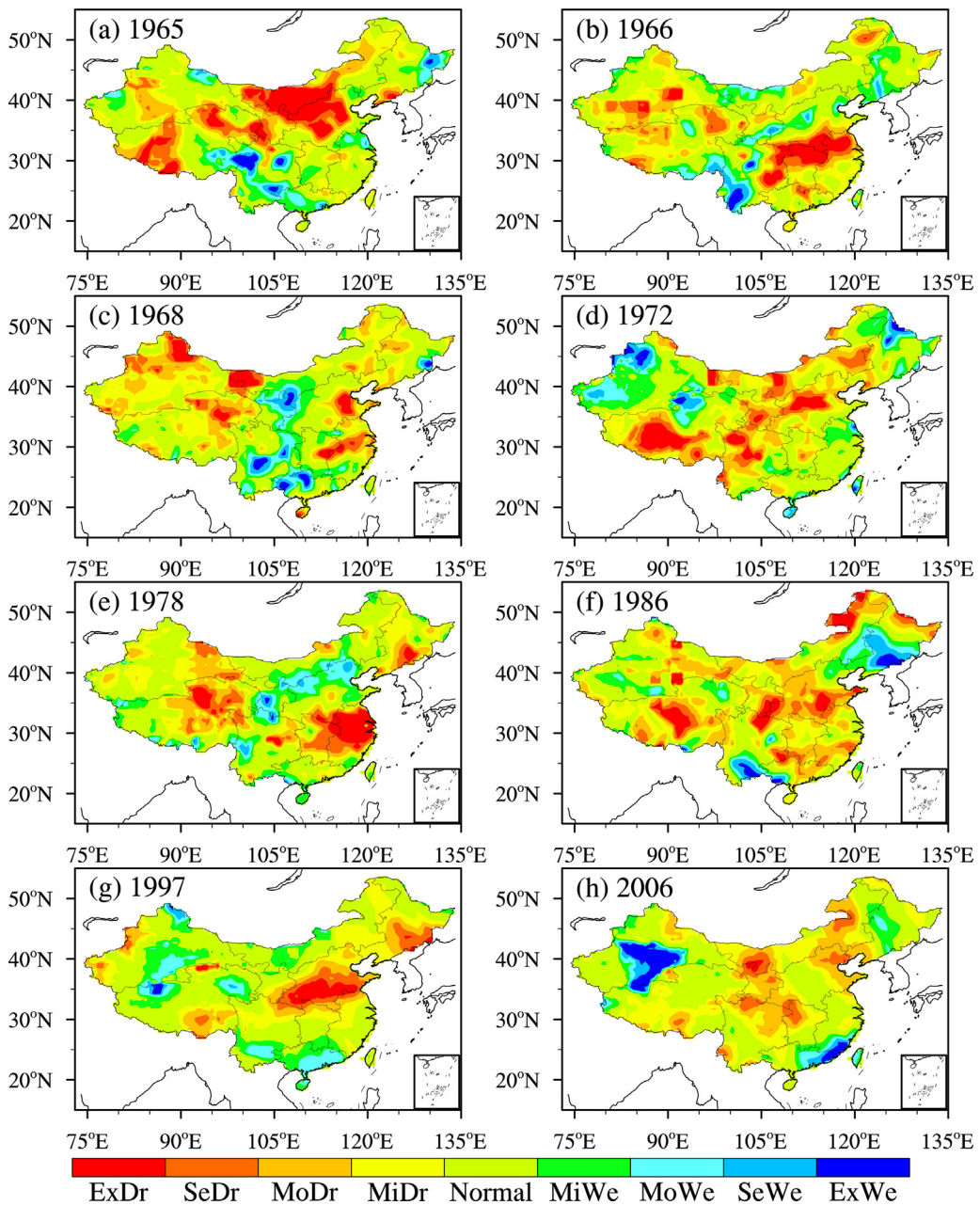


Fig. 3. Spatial distribution of drought severity over China in (a) 1965, (b) 1966, (c) 1968, (d) 1972, (e) 1978, (f) 1986, (g) 1997, and (h) 2006. (For definitions of the abbreviations regarding the drought severity classifications, see Table 1).

The reduction in the carbon fluxes (GPP and NEP) from CLM45-CN compared to those of CLM45-C can be explained as following. Since the C-N biogeochemistry is active, the amount of N required to support the potential growth is diagnosed in CLM45-CN, and GPP is reduced if N availability is insufficient to sustain the potential biomass increment. In contrast, CLM45-C uses a prescribed N factor, which varies among plant functional types, to represent N constraints on photosynthesis. Fig. 5 illustrates the difference in N limitation between the C-N coupling model and C-only model by presenting the spatial distribution of annual mean values of an instantaneous N limitation factor. This factor is the ratio of down-regulated GPP to potential GPP and expressed as a scalar ranging from 0 to 1, with values closer to 0 indicating stronger N limitation. It is seen that CLM45-CN (Fig. 5b) shows a stronger N limitation over the southeast, central and northeast parts of China, suggesting fewer amount of N than CLM45-C (Fig. 5a). Neverthe-

less, the changes in N limitation over other areas were small, on the order of $\pm 5\%$ (Fig. 5c). It suggests that the availability of mineral N in CLM45-CN is insufficient to maintain required plant C:N stoichiometry and sustain the potential biomass increment. Because canopy-level photosynthesis (or GPP) is derived by summing the sunlit and shaded leaf-level rates scaled by the sunlit and shaded leaf area indices and limited to the availability of mineral N. Unmet plant N demand is translated back to a carbon supply surplus which is eliminated through reduction of GPP, representing direct downregulation of photosynthetic rate under N limitation. The indirect N limitation effect of reduced allocation to new growth on light capture is another significant downregulation mechanism in the model, which operates on longer time scales and has a strong influence on global-scale plant-soil system states and fluxes (Thornton et al., 2007). It is noted that the reduction in GPP may lead to a decrease in LAI, which then induces a reduction in canopy evap-

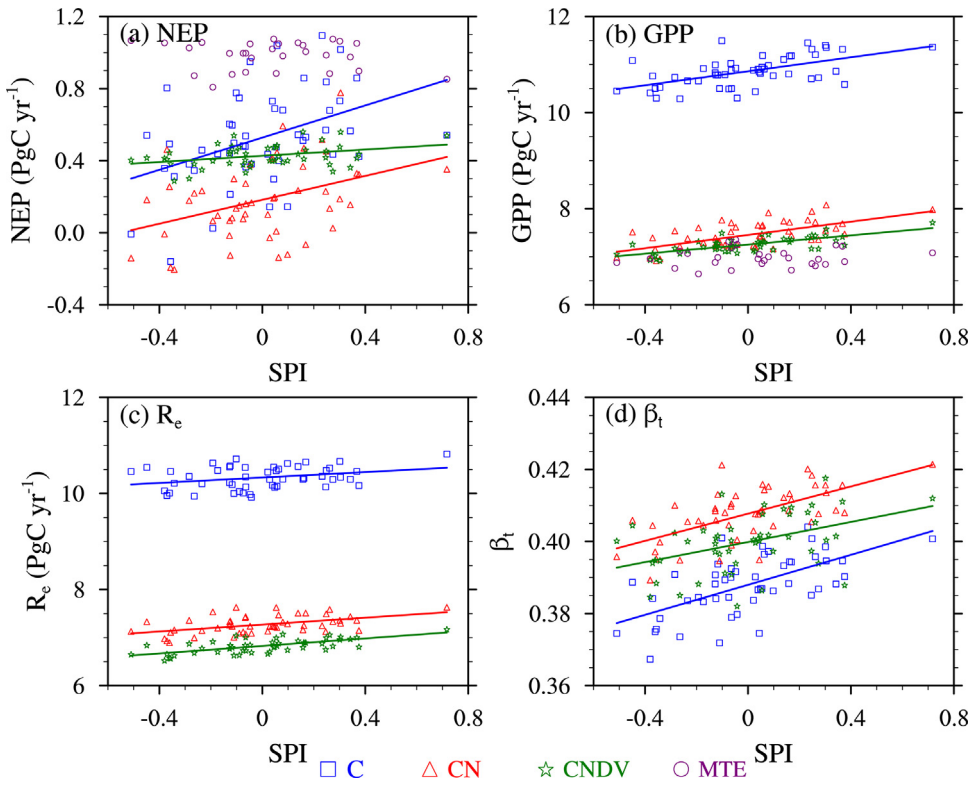


Fig. 4. Scatter plots between the annual mean SPI and total annual (a) NEP, (b) GPP, (c) R_e over China, and (d) soil water stress function (β_t) from 1961 to 2010. The annual SPI is the mean value of the 12-month SPI, through to the end of December over the whole of China.

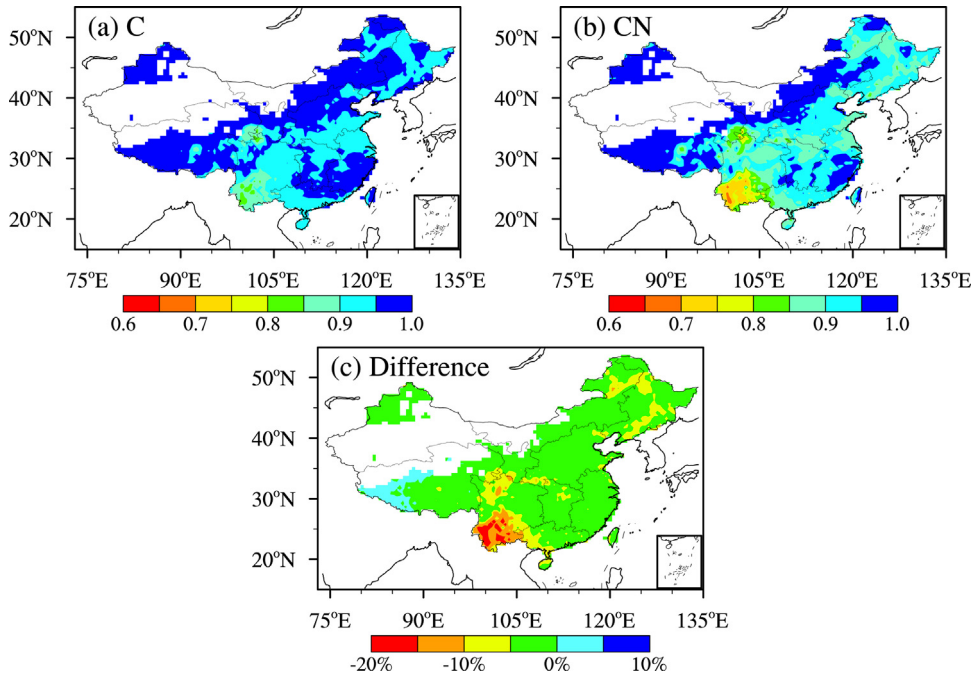


Fig. 5. Spatial distribution of instantaneous nitrogen limitation prescribed in (a) CLM45-C and predicted by (b) CLM45-CN. The values closer to 0 indicate stronger nitrogen limitation; areas with $\text{GPP} < 1 \text{ g m}^{-2} \text{ yr}^{-1}$ are shown in white.

transpiration (Oleson et al., 2013). Although the reduction in evapotranspiration may lead to an accumulation of soil water and increase the soil water stress function β_t (Fig. 4d) and thus increase N mineralization, the changes in soil water in tropical rainforest and boreal forest regions (e.g. over most parts of southern China) are insignificant (Lee et al., 2013). Therefore, decreasing canopy-

level photosynthesis due to the stronger N limitation in CLM45-CN would directly decrease the predicted national total GPP in China. In addition, lower N content in CLM45-CN also decreased autotrophic respiration because tissue N content is a suitable index of cellular metabolic rate (Oleson et al., 2013). The total heterotrophic demand for mineral N is in competition with the total plant N demand from

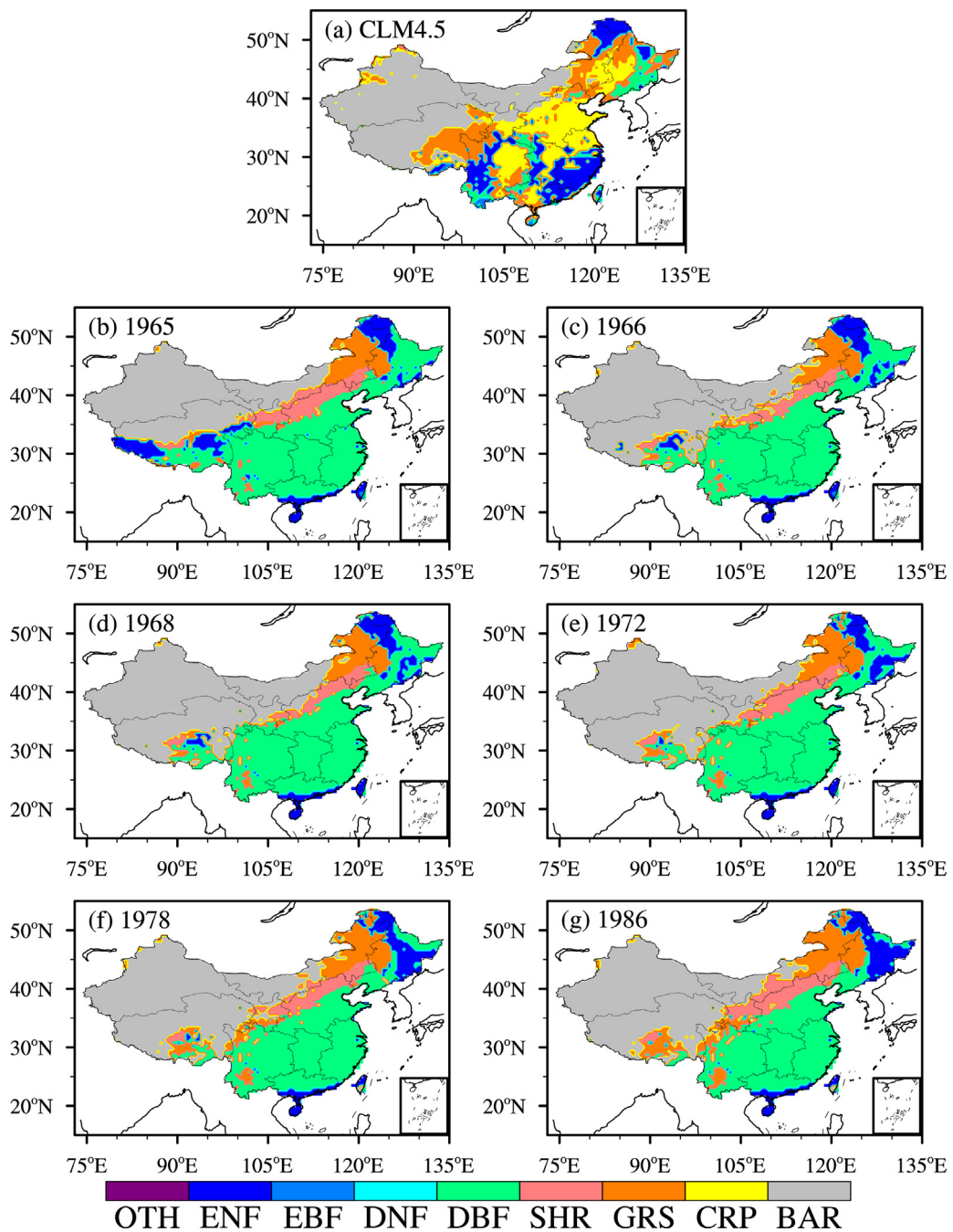


Fig. 6. Vegetation distribution from (a) the default map of CLM4.5, and the CLM45-CNDV simulations in (b) 1965, (c) 1966, (d) 1968, (e) 1972, (f) 1978, (g) 1986. The PFT information is shown in Table 2.

all PFTs sharing space on a single soil column. Limited mineral N in CLM45-CN also decreased the heterotrophic respiration. However, the reduction of R_e (Fig. 4c) has a smaller magnitude (Fig. 4c) than that of GPP, which then leads to a decrease of NEP in CLM45-CN compared to CLM45-C. Notably, the difference between the influences of the magnitude of N limitation and the dynamics of the internal N cycle on the response of the terrestrial carbon cycle to drought was not separated in this study.

The annual carbon flux predicted by the CLM45-CN simulation under drought conditions were relatively smaller than those from the CLM45-C simulation (Fig. 4 and S1). For example, the predicted total NEP in China in 1986 ($SPI = -0.51$) decreased by 0.53 PgC yr^{-1} and 0.32 PgC yr^{-1} in the CLM45-C and CLM45-CN simulations, respectively. Due to continuous water scarcity in 1965 ($SPI = -0.45$)

and 1966 ($SPI = -0.36$), a clear reduction in NEP was predicted for 1966 (Fig. S1a); NEP decreased by 0.69 PgC yr^{-1} and 0.37 PgC yr^{-1} for the CLM45-C and CLM45-CN simulations, respectively. The same results were obtained for GPP (Fig. S1b). In addition, under the drought conditions, less available soil water reduced nitrogen mineralization and increased nitrogen limitation (Felzer et al., 2011). This increased the correlation coefficient ($r = 0.67$) between the SPI and GPP anomalies (Fig. S1b) for CLM45-CN, compared with CLM45-C ($r = 0.62$). Meanwhile, since tissue N content has a close relationship with autotrophic respiration, the correlation between the SPI and R_e anomalies also increased in CLM45-CN (Fig. S1c). However, the correlation between SPI and NEP decreased, ($r = 0.51$ and 0.45 for CLM45-C and CLM45-CN, respectively). We have not identified a mechanism explaining the reduction in the sensitiv-

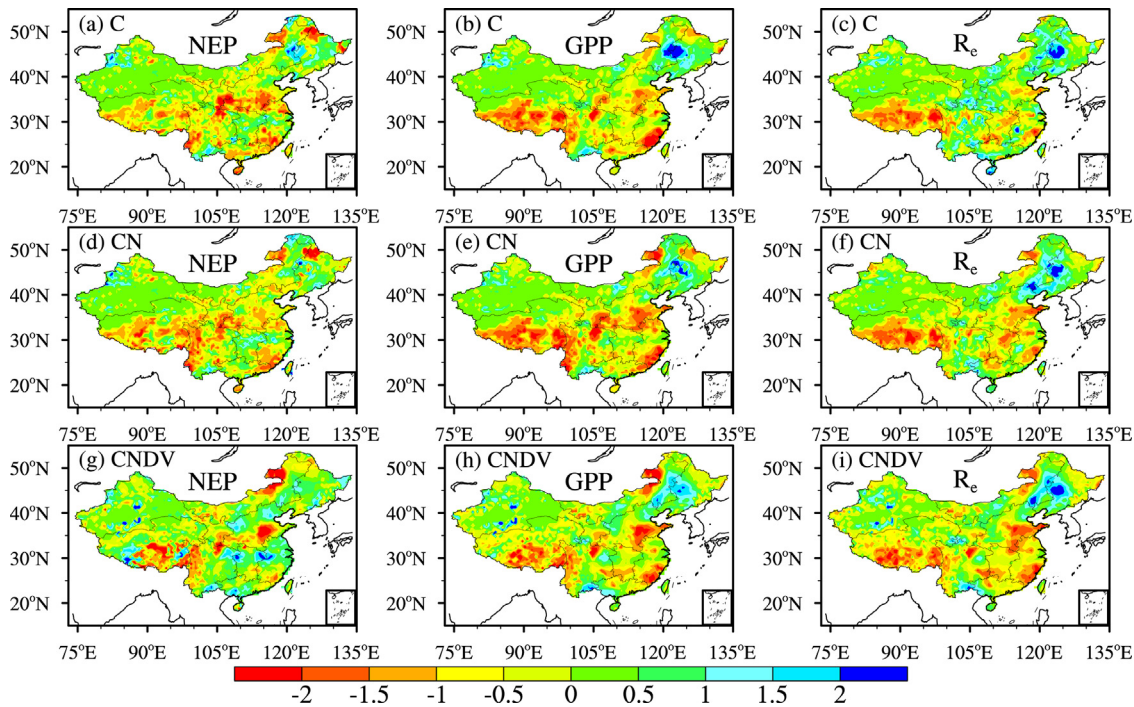


Fig. 7. Spatial distributions of the 1986 standardized anomaly index (SAI) values of annual net ecosystem production (NEP, left panels), gross primary production (GPP, central panels), and ecosystem respiration (R_e , right panels) for (a) CLM45-C, (b) CLM45-CN, and (c) CLM45-CNDV. Negative SAI values represent annual carbon fluxes smaller than the 50-year means; positive values represent fluxes greater than the 50-year means.

ity of NEP predictions to variation in precipitation in CLM45-CN compared to CLM45-C.

In general, compared to the default PFT map of CLM4.5 (used both in CLM45-C and CLM45-CN) (Fig. 6a, Table 2), the DV simulation in the CLM4.5 model produced a reasonably accurate vegetation distribution over northwest and northeast China; however, the predicted distribution over north and southeast China was less accurate (Fig. 6). Because CLM45-CNDV can simulate only unmanaged vegetation, the crop PFTs for the CLM45-C and CLM45-CN simulations over northern China were instead comprised of deciduous broadleaf trees. In addition, the incorporation of the DV model in CLM4.5 tended to decrease evergreen forests in the CLM45-CNDV simulation over southern China, which further reduced the mean (7.3 PgCyr^{-1}) and IAV (0.19 PgCyr^{-1}) of predicted GPP (Fig. 4b). Nevertheless, CLM45-CNDV predicted a slight increase in the NEP mean value (0.43 PgCyr^{-1}) compared to CLM45-CN (0.18 PgCyr^{-1}). These differences were due mainly to the different biogeography and mortality processes. CLM45-CNDV changes the CN framework only as needed to simulate biogeography, which induces the differences of the PFT distribution (Fig. 6). Moreover, CLM45-CN assumes the whole-plant mortality to be a constant rate of $2\% \text{ yr}^{-1}$ for all vegetation types. In contrast, CLM45-CNDV calculates the gap mortality based on heat stress and growth efficiency. The different mortality algorithm of CLM45-CNDV resulted in lower vegetation mortality compared to CLM45-CN (Gotangco Castillo et al., 2012). Thus, the CLM45-CNDV simulation maintained more total vegetation carbon and generated less litter and soil carbon than the CLM45-CN simulation, which in turn reduced heterotrophic respiration to give higher NEP. The intensity of the predicted change in GPP induced by drought also was dampened by the DV model. For example, the total GPP in China, according to the CLM45-CNDV simulation, decreased by only 0.3 PgC yr^{-1} and 0.2 PgCyr^{-1} in 1966 and 1986, respectively, compared to reductions of 0.53 PgCyr^{-1} and 0.46 PgCyr^{-1} in the CLM45-CN simulation. Further, because the spatio-temporal variations of the DV distribution had a stronger

response to the atmospheric forcing data due to the incorporation of the DV model than did the static vegetation distribution in the CLM45-C or CLM45-CN simulations, the SPI contributed more to the GPP anomalies ($r=0.74$) and R_e ($r=0.68$). But, CLM45-CNDV showed a weak relationship between the soil water stress function β_t and drought index SPI ($r=0.42$) while the CLM45-C ($r=0.64$) and CLM45-CN ($r=0.63$) showed similar correlation coefficients between these two parameters (Fig. S1d).

Compared to the MTE data between 1982 and 2010, all three CLM4.5 configurations captured the temporal variation of GPP well before 2002, but showed large discrepancies thereafter (Fig. S1b). The CLM45-C overestimated the mean of total GPP in China (10.9 PgCyr^{-1}), while CLM45-CN (7.5 PgCyr^{-1}) and CLM45-CNDV (7.3 PgCyr^{-1}) predicted GPP that was closer to the MTE dataset (7.0 PgCyr^{-1}). In addition, CLM45-C (0.32 PgCyr^{-1}) and CLM45-CN (0.27 PgCyr^{-1}) overestimated the IAV in GPP compared to the MTE data (0.19 PgCyr^{-1}), while the CLM45-CNDV simulation (0.18 PgCyr^{-1}) showed a slight underestimation. Since no NEP observations were available, the NEE data from MTE were used to evaluate the CLM4.5 simulations by multiplying the NEE data by a factor of -1.0 ; however, the accuracy for this transformation may have been affected by some disturbances, e.g. biomass burning or land use (Oleson et al., 2013). The IAV of NEP in Chinese terrestrial ecosystems between 1982 and 2010 was predicted to be 0.26 , 0.21 and 0.06 PgCyr^{-1} by the CLM45-C, CLM45-CN, and CLM45-CNDV simulations, respectively, compared to 0.08 PgCyr^{-1} for the MTE data. It is noted that current attempts to produce maps of NEE from flux towers have been much less successful than for GPP (Jung et al., 2011).

3.3. Carbon cycle extremes in China's terrestrial ecosystems

As the most severe drought over the past 50 years occurred in 1986 (Fig. 3f), the corresponding spatial distribution of the SAI for the terrestrial ecosystem carbon fluxes (NEP, GPP, R_e) (Fig. 7) was of particular interest. The predicted GPP mainly decreased over most

Table 2

Typical plant functional types (PFTs) used in this study and their corresponding PFTs in the CLM4.5 model.

	Abbr.	PFT in this study	PFT in CLM45
1	ENF	Evergreen needleleaf forest	Needleleaf evergreen tree (temperate, boreal)
2	EBF	Evergreen broadleaf forest	Broadleaf evergreen tree (tropical, temperate)
3	DNF	Deciduous needleleaf forest	Needleleaf deciduous tree (boreal)
4	DBF	Deciduous broadleaf forest	Broadleaf deciduous tree (tropical, temperate, boreal)
5	SHR	Shrubland	Broadleaf evergreen shrub (temperate); Broadleaf deciduous shrub (temperate, boreal)
6	GRS	Grassland	C3 arctic grass; C3 grass; C4 grass
7	CRP	Cropland	Crop
8	BAR	Bare soil	Bare soil
9	OTH	Water or Urban	Glacier; Lake; Wetland; or Urban

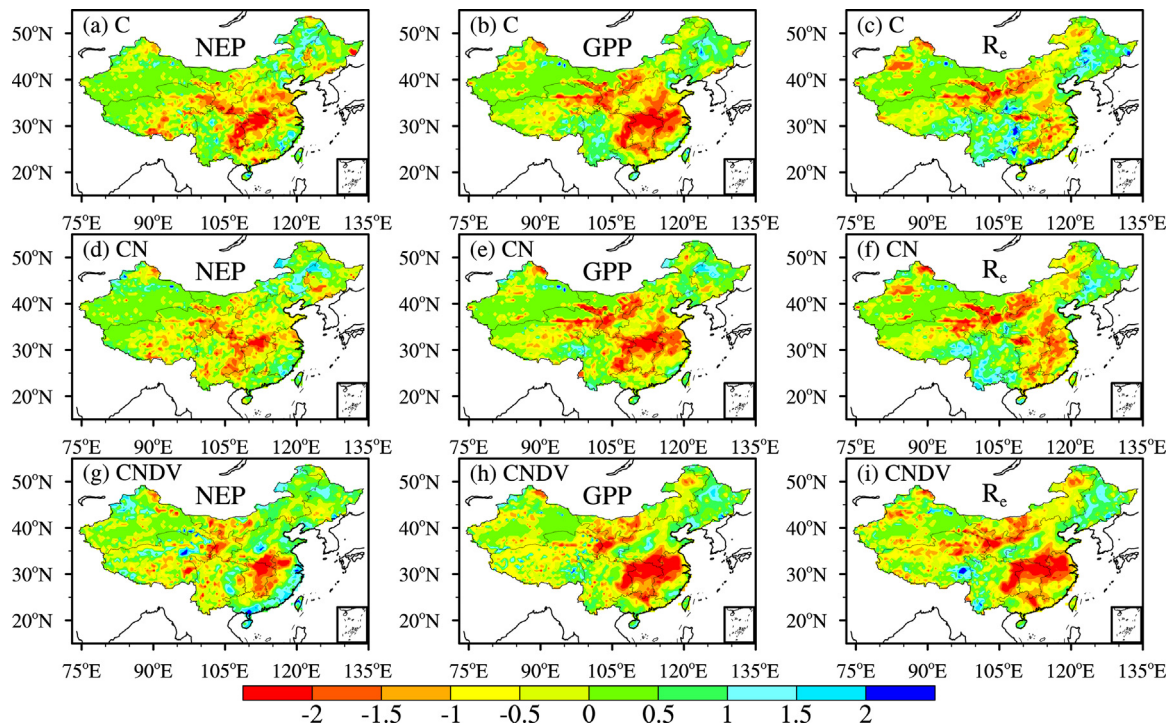


Fig. 8. Spatial distributions of the 1966 standardized anomaly index (SAI) values of annual net ecosystem production (NEP, left panels), gross primary production (GPP, central panels), and ecosystem respiration (R_e , right panels) for (a) CLM45-C, (b) CLM45-CN, and (c) CLM45-CNDV. Negative SAI values represent annual carbon fluxes smaller than the 50-year means; positive values represent fluxes greater than the 50-year means.

of the Tibetan Plateau, and parts of southwest, southeast and northern China (Fig. 7, middle panel); in these areas, there was also a clear decrease in ecosystem respiration (Fig. 7, right panel). Compared to GPP and R_e , there were large differences in the NEP predictions among the spatial patterns produced by the three CLM4.5 configurations. Fewer areas experienced the extreme decrease in carbon sequestration (NEP) according to the CLM45-CNDV simulation, compared to the CLM45-C and CLM45-CN simulations.

Although the drought events in 1965 (Fig. 3a) and 1966 (Fig. 3b) were not the most severe, continuous water scarcity led to the greatest reduction in vegetation productivity of all the years in 1966 (Fig. 8). The decrease in GPP mainly occurred in the central areas of China (Fig. 8, middle panel) and the three CLM4.5 configurations produced similar spatial patterns, except for lower SAIs simulated by CLM45-CNDV. However, the CLM45-CNDV simulation showed a greater decrease in R_e over central and southeast China due to differences in the representation of vegetation types in three model configurations. This area is mainly covered by crop and evergreen needleleaf forest for the fixed PFT in the CLM45-C and CLM45-CN simulations (Fig. 6a), but by deciduous broadleaf forest in the CLM45-CNDV simulation (Fig. 6).

3.4. The lagged effects of drought on GPP and NEP

Drought not only has immediate effects on the carbon cycle, but also can initiate lagged responses (Pei et al., 2013; Reichstein et al., 2013). As shown in Fig. 9, for the past 50 years the SAI of simulated GPP (GPP_{SAI}) was closely correlated with the SPI over southern China ($r > 0.6, p < 0.05$), especially over cropland and grassland regions. The accumulative lagged effect of drought on the GPP_{SAI} occurred over relatively short timescales (e.g., 1–3 months) over most areas of southern and central China; over the Tibetan Plateau, southwest China and northwest China the NEP responded to drought over longer timescales (6–12 months). The CLM45-CN simulation (Fig. 9d) predicted a similar response to drought as the CLM45-C simulation (Fig. 9b). In contrast, the DV model triggered a stronger response, with higher correlations in northern and northeast China (Fig. 9e) and longer timescales in Qinghai Province (Fig. 9f). These differences further prove that the inclusion of both interactive N and DV simulations in the CLM4.5 model yields a stronger response of GPP to drought, compared to inclusion of the interactive N simulation alone; this may be because the CNDV configuration is able to adjust the response according to both the

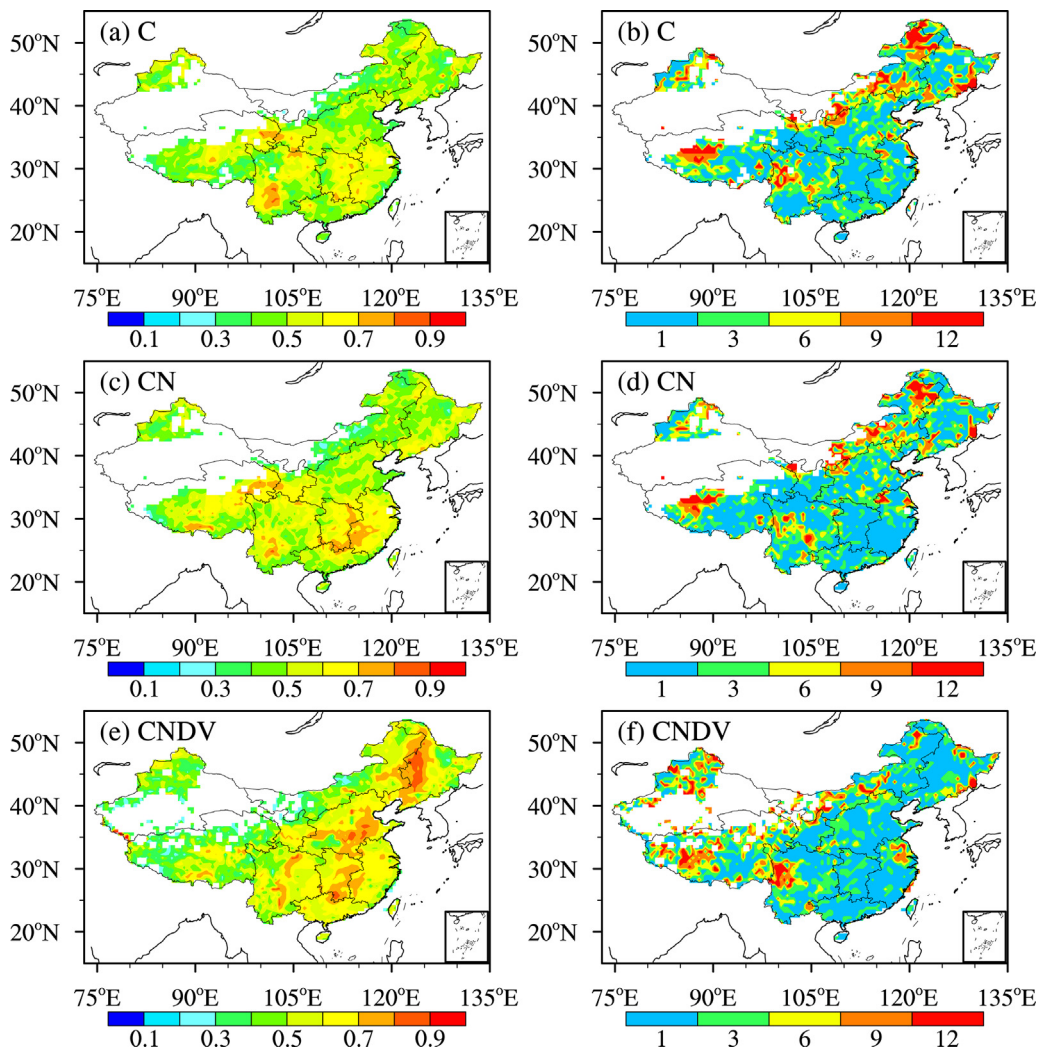


Fig. 9. Spatial distributions of the maximum correlation coefficients (left panels) between the standardized precipitation index (SPI) at different timescales (1-, 3-, 6-, 9- and 12-month), and monthly standardized anomaly index of predicted gross primary production (GPP_{SAI}) and their corresponding timescales (right panels), for the CLM45-C, CLM45-CN, and CLM45-CNDV simulations, respectively. Areas with insignificant correlations ($p < 0.05$) are indicated in white.

nitrogen–carbon interaction and the establishment (and mortality) of vegetation (Fig. 6).

The NEP is a balance between GPP and R_e , so the complex relationship between R_e and the SPI led to a weaker correlation between the NEP_{SAI} and the SPI, compared to that between GPP and SPI (Fig. 10). The maximum correlation coefficients for the CLM45-CNDV simulation mainly occurred over the Tibetan Plateau and Inner Mongolia (Fig. 10a and c), and also across northern and northeast China (Fig. 10e). Compared to GPP_{SAI}, NEP_{SAI} was not significantly correlated with the SPI ($p < 0.05$) over many vegetation-covered areas of southern China (Fig. 10, left panel). In addition, drought had a longer lagged effect on NEP than on GPP (Fig. 10, right panel).

4. Discussion

4.1. Effects of climate conditions and vegetation types

Previous studies have pointed out that the effects of drought on terrestrial ecosystems are dependent on the vegetation types and climate regions (Liu et al., 2014; Pei et al., 2013; Reichstein et al., 2013). For the three CLM4.5 simulations, the anomalies of annual GPP and R_e were significantly correlated with the annual mean SPI ($p < 0.05$) over all of the sub-regions in China (Fig. 11). The

response of GPP to drought was relatively strong ($r > 0.6$) over most of the nine sub-regions (Fig. 11a). Both the CLM45-CN and CLM45-CNDV simulations increased the correlations of GPP with annual SPI, compared to the CLM45-C simulation. The comparatively lower correlations in southwest China may have occurred because ample water is usually available for the vegetation growth in this area, while radiation is an important climate driver of GPP (Jia et al., 2013b; Nemani et al., 2003).

There were significant discrepancies in the simulated response of R_e to drought among the three CLM4.5 configurations (Fig. 11b). Compared to the CLM45-C simulation, the CLM45-CN simulation produced higher correlations of R_e with annual SPI; the incorporation of the DV model further strengthened the predicted response to drought, which is consistent with the results shown in Fig. S1. The SAIs of predicted NEP for the three simulations showed positive and significant correlations with the annual SPI over arid and semiarid regions (regions R2, R3, and R4), as well as in northeast China (R1), but the correlations were not significant over southwest China (Fig. 11c). In addition, the NEP anomalies from the CLM45-CNDV simulations were not significantly correlated with the annual SPI over central and southern parts of China (R5, R7, and R8).

Overall, the predicted anomalies of annual GPP and R_e were significantly correlated with the annual mean SPI ($p < 0.05$) over all of the PFTs. Notably, there is no evergreen needleleaf forest based on

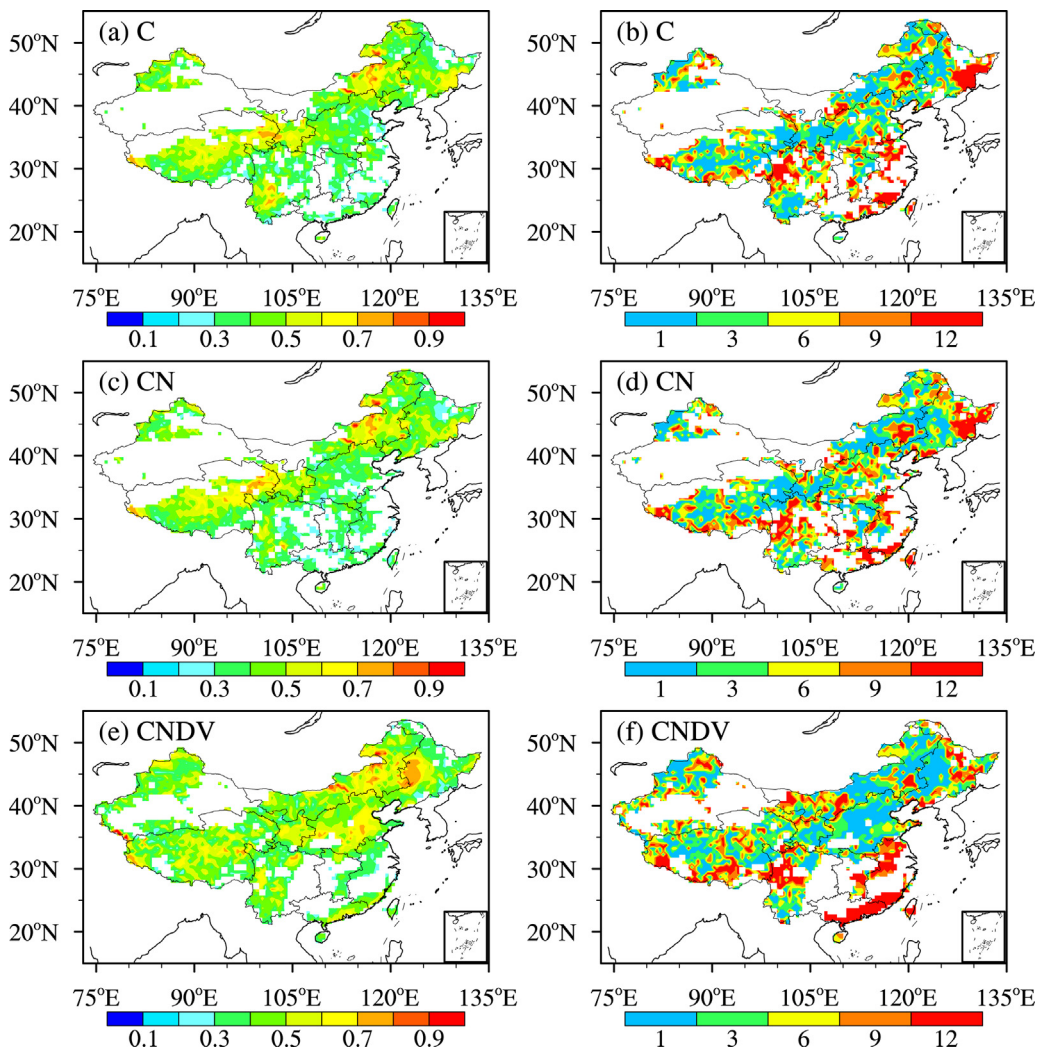


Fig. 10. Spatial distributions of the maximum correlation coefficients (left panels) between the standardized precipitation index (SPI) at different timescales (1-, 3-, 6-, 9- and 12-month), and monthly standardized anomaly index of predicted net ecosystem production (NEP_{SAI}) and their corresponding timescales (right panels), for the CLM45-C, CLM45-CN, and CLM45-CNDV simulations, respectively. Areas with insignificant correlations ($p < 0.05$) are indicated in white.

the CLM4.5 surface data set in China in the CLM45-CNDV simulation (Fig. 6) or in simulations that exclude the DV model (Fig. 1b). Compared to other PFTs, the GPP of the evergreen broadleaf forest had a lower correlation with SPI (Fig. 12a), and a similar response can be seen for R_e (Fig. 12b). These results indicate that water may not be the most important climate factor controlling evergreen broadleaf forest (Liu et al., 2014), which exists mainly over southern China (Fig. 1b), while radiation dominantly drives its IAV of productivity of this PFT (Jia et al., 2013b; Nemani et al., 2003). In addition, both croplands and grasslands were predicted to have higher correlations between the annual mean NEP anomalies and the SPI (Fig. 12c). The effects of human activities (e.g., irrigation, grazing) were not taken into consideration in this study, yet the two vegetation types do not have much capability in resisting severe drought and they are water sensitive. For example, they cannot obtain water from deeper soil layers with their shadow roots during the drought period compared with forest ecosystems and thus the NEP would be greatly reduced (Wu and Chen, 2013). When sufficient soil moisture and favorable temperatures are available, the NEP also tends to respond more rapidly. This high sensitivity has been demonstrated in previous studies (Huxman et al., 2004; Wu and Chen, 2013). To further investigate the effect of interactive N cycle on the response of terrestrial ecosystem carbon cycle to drought across PFTs, we examined the relationship between the total N mineralization flux

and soil water stress function β_t for 6 PFTs over China (Fig. 13). It is seen that CLM45-CN has lower N mineralization than CLM45-C for all PFTs, which suggests that the incorporation of interactive N cycle clearly reduces the availability of N mineralization and thus induces the reductions of GPP and R_e (Fig. 4 and S1). Fig. 13 also shows that the N mineralization decreases with the decrease of soil water stress function β_t (e.g., intensification of drought) for both CLM45-C and CLM45-CN over all PFTs except the EBF (Fig. 13b). The reason is similar to that for the carbon fluxes (Fig. 12), which may be due to that evergreen broadleaf forest exists mainly over southern China (Fig. 1b) where soil moisture is sufficient (Nemani et al., 2003; Jia et al., 2013b; Liu et al., 2014). In addition, the correlations between the N availability and soil water availability for CLM45-CN are higher over all PFTs than those for CLM45-C except the EBF. This confirms that the carbon-nitrogen coupling increases the relationship between the N mineralization and soil water and thus strengthens the predicted response of GPP to drought (Fig. S1).

4.2. Impacts of drought intensity

To better understand the drought sensitivities of the three model configurations, responses to three levels of drought (25, 50 and 75% reductions in precipitation) were examined through two ideal site-level drought experiments located in temperate

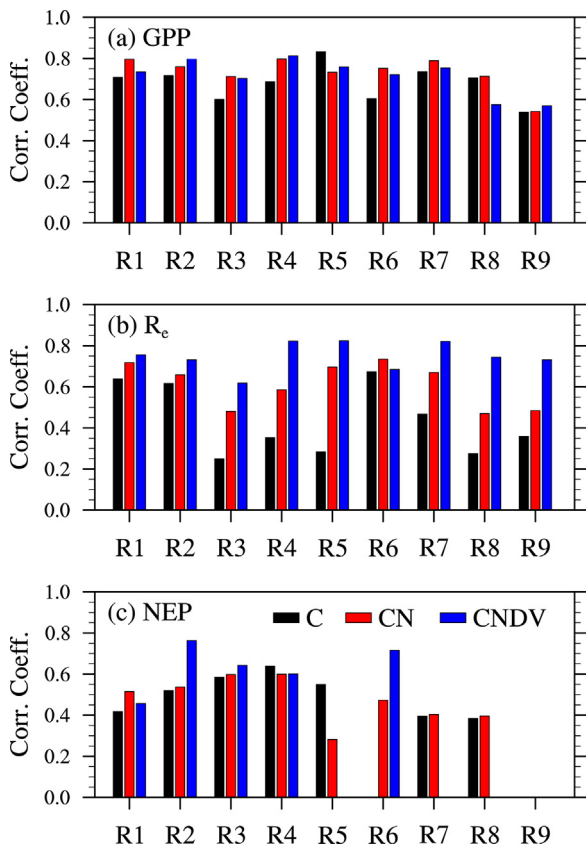


Fig. 11. The correlation coefficients between the annual standardized precipitation index (SPI) and standardized anomaly index (SAI) of (a) gross primary production (GPP), (b) ecosystem respiration (R_e) and (c) net ecosystem production (NEP) for the CLM45-C, CLM45-CN, and CLM45-CNDV simulations, over each of the nine sub-regions (shown in Fig. 1a) in China.

deciduous forest ($51.25^{\circ}\text{N}, 126.75^{\circ}\text{E}$) and grass ($46.25^{\circ}\text{N}, 116.25^{\circ}\text{E}$) ecosystems, respectively. The three configurations (CLM45-C, CLM45-CN, and CLM45-CNDV) were compared to determine the level of the agreement in the timing and magnitude of the predicted responses of ecosystem carbon fluxes to different levels of drought (Fig. 14). All model simulations followed a standardized spin-up, similar to that described in Section 2.2, and were initialized from these spin-ups followed by three years (2003–2005) of reduced precipitation for each site. The three drought levels (25, 50 and 75% reductions in precipitation) are denoted hereafter as d25, d50 and d75, respectively, while d0 identifies the control simulation under observed precipitation (0% reduction). Notably, precipitation was reduced all year, but other meteorological variables were not manipulated. The incorporation of interactive N and DV simulations decreased predicted GPP and NEP under different drought levels at both sites (Fig. 14), compared to the simulation with the basic CLM4.5 model. As drought intensity increased, there was increasing disagreement in the magnitude of carbon fluxes predicted by the basic and amended CLM4.5 models. For the grass ecosystem, the discrepancy between CLM45-C and CLM45-CN became smaller as drought intensity increased (e.g., d50 and d75; Fig. 13d and f). Compared to the forest PFT, grass showed a quicker decrease in GPP, suggesting that it is more sensitive to drought due to relatively short roots.

4.3. Uncertainties of the CLM4.5 simulations

As described in Section 3.2 and shown in Fig. 4, CLM45-C overestimated the mean and IAV of GPP compared to the MTE data.

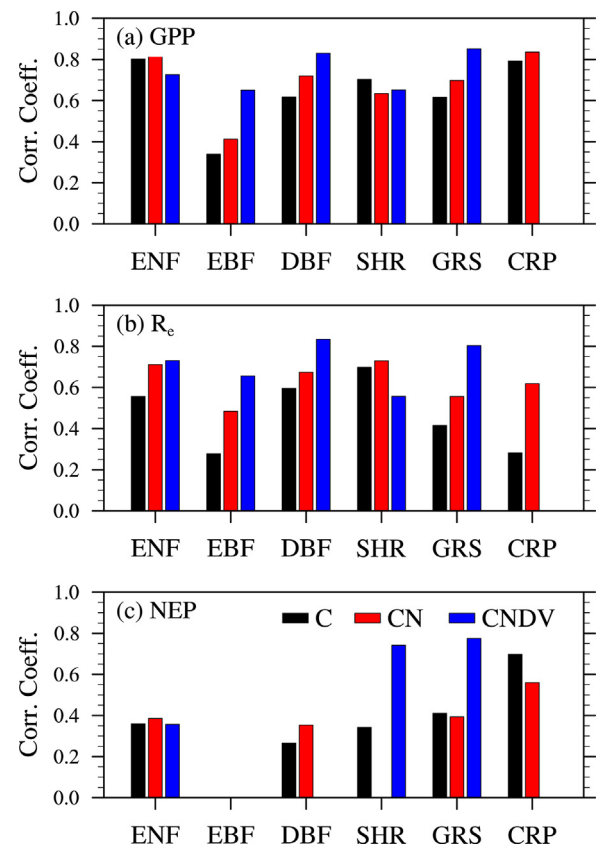


Fig. 12. The correlation coefficients between the annual standardized precipitation index (SPI) and standardized anomaly index (SAI) of (a) gross primary production (GPP), (b) ecosystem respiration (R_e) and (c) net ecosystem production (NEP) for the CLM45-C, CLM45-CN, and CLM45-CNDV simulations for six plant functional types (PFTs) (See Table 2 for PFT definitions).

In contrast, the incorporation of the interactive N cycle simulation into CLM4.5 decreased the mean and IAV of predicted GPP by 31% and 16%, respectively; the addition of the DV model led to a further reduction of 3% and 33% in the mean and IAV of predicted GPP, respectively. These results suggest that the inclusion of interactive N (i.e., modifying CLM45-C to CLM45-CN) has greater impact on the averaged values of predicted GPP than does the further addition of the DV model (i.e., modifying CLM45-CN to CLM45-CNDV). For carbon sequestration by the terrestrial ecosystems (i.e., NEP) in China, CLM45-C and CLM45-CN overestimated the IAV while CLM45-CNDV showed a slight underestimation, compared to the MTE data (Jung et al., 2011). In fact, the average NEP in China predicted by the CLM45-C, CLM45-CN and CLM45-CNDV models was 0.52, 0.18, and 0.42 PgCyr^{-1} , respectively. The CLM45-CN simulation is comparable to the results from five process-based ecosystem models (Piao et al., 2009), which produced NEP estimates ranging from 0.13 PgCyr^{-1} to 0.22 PgCyr^{-1} with an average of $0.173 \pm 0.039 \text{ PgCyr}^{-1}$. The CLM45-C and CLM45-CNDV models overestimated NEP compared to the results of Piao et al. (2009). It is noted that the analysis of the carbon-nitrogen coupling is subject to some limitations in the present study. Nitrogen deposition and application increased significantly in China during recent decades, which might regulate the terrestrial carbon cycle in China, but these factors were not considered in this paper.

5. Summary

In this study, the effects of incorporating the interactive N and dynamic vegetation simulations in the process-based land surface

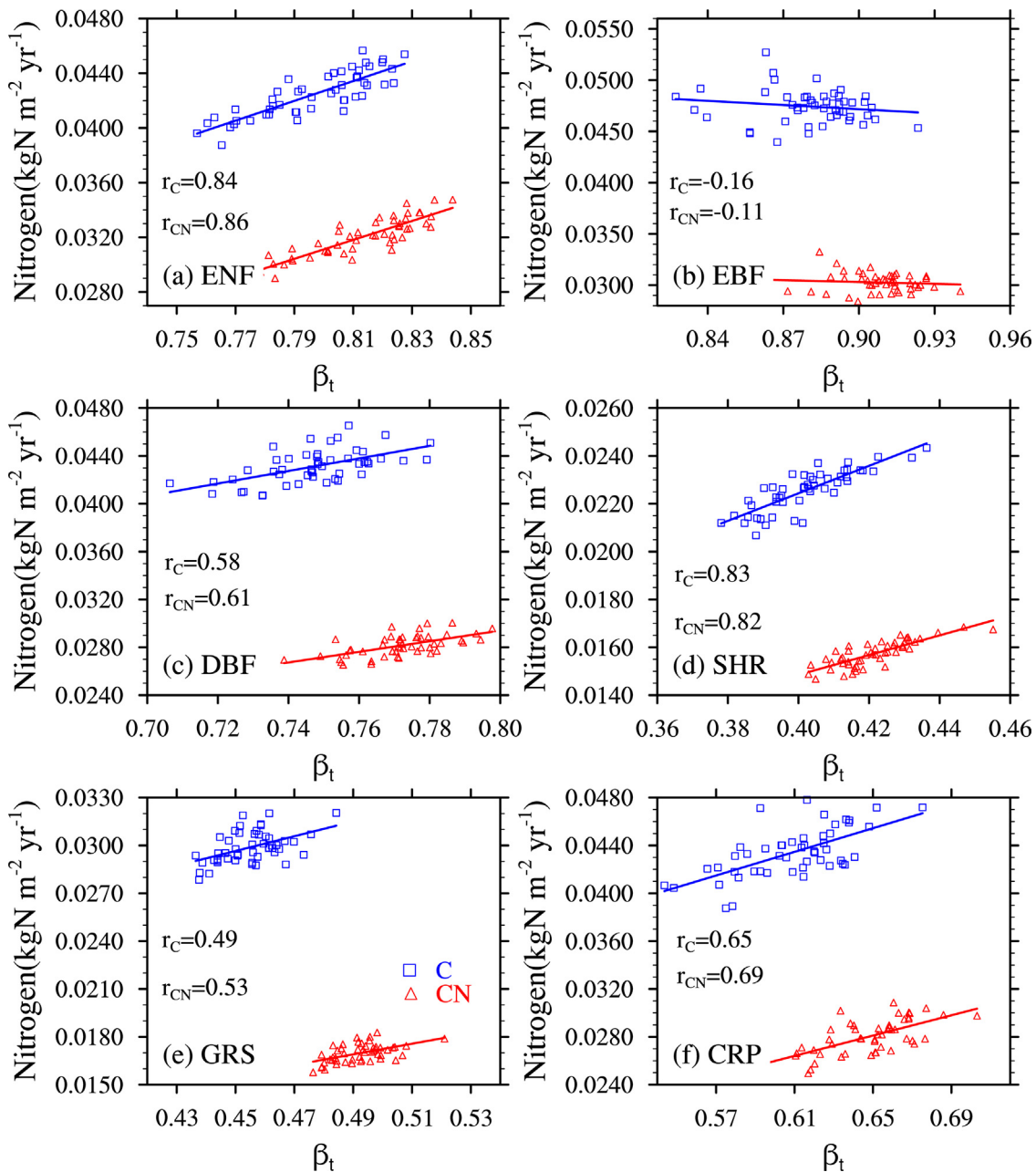


Fig. 13. Relationship between nitrogen flux and soil water stress function (β_t) for six plant functional types (PFTs) (See Table 2 for PFT definitions). The r_C and r_{CN} represent their temporal correlation coefficients for CLM45-C and CLM45-CN, respectively.

model, CLM4.5, were investigated. Specifically examined were the effects on the predicted response of the terrestrial carbon cycle across China to drought. As indicated by the SPI, China experienced several drought events with different intensities and areal extents from 1961 to 2010; especially notable years include 1965, 1966, 1968, 1972, 1978 and 1986, in which the SPI < -0.35 and more than 24% of the total area in China was affected by either moderate, severe or extreme drought. Due to the continuous scarcity of soil water across 1965 and 1966, the total predicted NEP of China declined by 0.69 PgCyr^{-1} and 0.37 PgCyr^{-1} in 1966, according to the CLM45-C and CLM45-CN simulations, respectively.

Compared to the default PFT map of CLM4.5, the CLM45-CNDV produced a similar vegetation distribution over northwest and northeast China except the differences over southern China, where the deciduous forest was observed in CLM45-CNDV instead of the evergreen needleleaf forest. In general, incorporating the

interactive N and DV into the CLM4.5 model mostly reduced the annual means and IAV of the simulated terrestrial carbon fluxes (i.e., GPP and NEP), except for a slight increase in the NEP mean value predicted by CLM45-CNDV (0.43 PgCyr^{-1}) compared to that by CLM45-CN (0.18 PgCyr^{-1}). This difference was mainly due to CLM45-CNDV's different mortality algorithm (based on heat stress and growth efficiency). Compared to the MTE data (7.0 PgCyr^{-1}) between 1982 and 2010, CLM45-C overestimates the annual GPP of the terrestrial ecosystems over China (10.9 PgCyr^{-1}), while CLM45-CN (7.5 PgCyr^{-1}) and CLM45-CNDV (7.3 PgCyr^{-1}) have lower biases. In addition, CLM45-C (0.32 PgCyr^{-1}) and CLM45-CN (0.27 PgCyr^{-1}) overestimate the IAV in GPP compared to the MTE data (0.19 PgCyr^{-1}), while the CLM45-CNDV simulation (0.18 PgCyr^{-1}) shows a slight underestimation.

The carbon-nitrogen coupling strengthened the predicted response of GPP to drought, yielding a higher correlation with

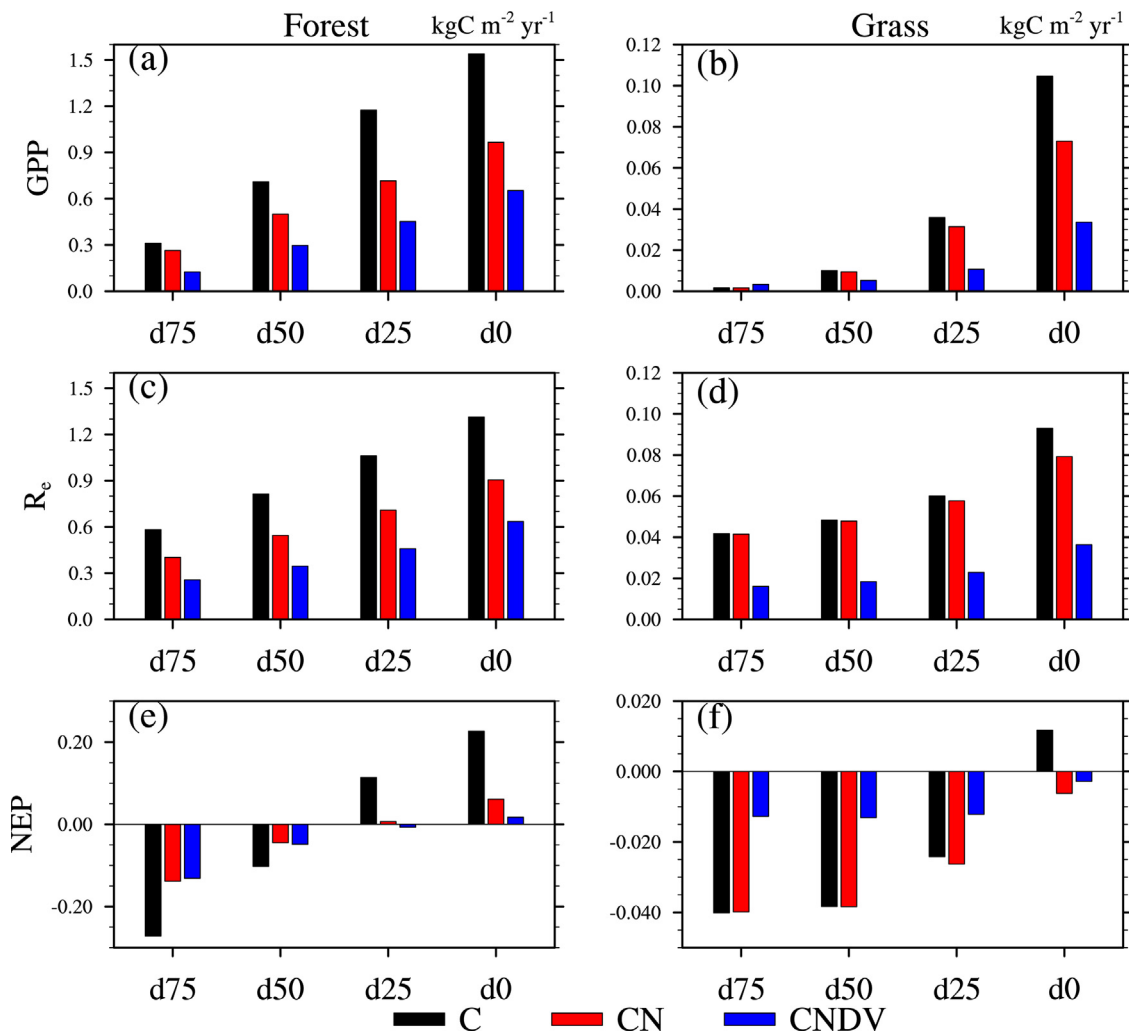


Fig. 14. Three-year averaged ecosystem carbon fluxes (gross primary production (GPP), ecosystem respiration (R_e) and net ecosystem production (NEP)) for the CLM45-C, CLM45-CN, and CLM45-CNDV simulations in temperate deciduous forest (left side) and grass (right side) ecosystems. Drought intensities are indicated by d75, d50, d25 and d0 which are, respectively, 75, 50, 25, and 0% reductions in precipitation.

SPI ($r_C = 0.62$, $r_{CN} = 0.67$), but a weaker sensitivity of NEP to SPI ($r_C = 0.51$, $r_{CN} = 0.45$). Results also showed that drought has an accumulative, lagged effect on GPP and that CLM45-CNDV predicted the longest lagged responses among the three CLM4.5 configurations. The lagged effects on GPP occurred over relatively shorter timescales in humid and warm areas (e.g., southern and central China) and over longer timescales across the Tibetan Plateau. In contrast, the predicted response of the NEP to drought was not significant over many vegetation-covered areas, and the lagged effect occurred over longer timescales because ecosystem respiration had a complex relationship with drought.

This study provides an indication of the impacts of drought on the terrestrial carbon cycle, with or without the use of interactive N and vegetation dynamics. The results can provide insight into how the CLM4.5 model predicts different response of the terrestrial carbon cycle to drought depending on whether simulations incorporate the interactive N and DV. Due to limited observations, however, the present study did not examine which version of the model could better simulate vegetation response to drought. In addition, although certain results from the present work are model specific, this approach can be applied to compare the impacts of drought on terrestrial carbon cycle using carbon-only models versus prognostic carbon–nitrogen models, or models with static versus dynamic vegetation.

Acknowledgments

This research was supported by the National Key Research and Development Program of China (2016YFA0600203), the Project PAEKL-2018-C5 supported by Open Research Fund Program of Plateau Atmosphere and Environment Key Laboratory of Sichuan Province, the Key Research Program of Frontier Sciences, CAS (QYZDY-SSW-DQC012), the National Natural Science Foundation of China (Grant Nos. 41575096, 41405083 and 91437220), and Natural Science Foundation of Hunan Province (Grant No. 2015JJ3098). We would particularly like to thank Dr. Yibo Liu for his helpful discussions. The CRUNCEP and MTE data were downloaded freely from the National Center for Atmospheric Research (<http://www.cesm.ucar.edu/>) and the Max Plank Institute for Biogeochemistry (<https://www.bgc-jena.mpg.de/>), respectively. The authors would like to thank the editor and the reviewers for their constructive comments and suggestions on the paper.

Appendix A. Supplementary data

Supplementary data associated with this article can be found, in the online version, at <https://doi.org/10.1016/j.ecolmodel.2017.11.009>.

References

- Bonan, G.B., Levis, S., 2010. Quantifying carbon-nitrogen feedbacks in the community land model (CLM4). *Geophys. Res. Lett.* 37, L07401, <http://dx.doi.org/10.1029/2010GL042430>.
- Bonan, G.B., Lawrence, P.J., Oleson, K.W., Levis, S., Jung, M., Reichstein, M., Lawrence, D.M., Swenson, S.C., 2011. Improving canopy processes in the Community Land Model (CLM4) using global flux fields empirically inferred from FLUXNET data. *J. Geophys. Res.* 116, G02014, <http://dx.doi.org/10.1029/2010JG001593>.
- Chen, H., Dickinson, R.E., Dai, Y., Zhou, L., 2011. Sensitivity of simulated terrestrial carbon assimilation and canopy transpiration to different stomatal conductance and carbon assimilation schemes. *Clim. Dyn.* 36, 1037–1054, <http://dx.doi.org/10.1007/00382-0010-00741-00382>.
- Collatz, G.J., Ball, J.T., Grivet, C., Berry, J.A., 1991. Physiological and environmental regulation of stomatal conductance, photosynthesis and transpiration: a model that includes a laminar boundary layer. *Agric. For. Meteorol.* 54, 107–136, [http://dx.doi.org/10.1016/0168-1923\(91\)90002-8](http://dx.doi.org/10.1016/0168-1923(91)90002-8).
- Dai, A., 2013. Increasing drought under global warming in observations and models. *Nat. Clim. Change* 3 (1), 52–58.
- Delire, C., Foley, J.A., Thompson, S.L., 2004. Long-term internal variability in a coupled atmosphere-biosphere model. *J. Climate* 17, 3947–3959.
- Felzer, B.S., Cronin, T.W., Melillo, J.M., Kicklighter, D.W., Schlosser, C.A., Dangal, S.R.S., 2011. Nitrogen effect on carbon-water coupling in forests, grasslands, and shrublands in the arid western United States. *J. Geophys. Res.* 116, G03023, <http://dx.doi.org/10.1029/2010JG001621>.
- Gotangco Castillo, C., Levis, S., Thornton, P., 2012. Evaluation of the new CNVD option of the Community Land Model: effects of dynamic vegetation and interactive nitrogen on CLM4 means and variability. *J. Climate* 25, 3702–3714, <http://dx.doi.org/10.1175/JCLI-D-11-00372.1>.
- Huxman, T.E., Smith, M.D., Fay, P.A., Knapp, A.K., Shaw, M.R., Loik, M.E., Smith, S.D., Tissue, D.T., Zak, J.C., Weltzin, J.F., Pockman, W.T., Sala, O.E., Haddad, B., Harte, J., Koch, G.W., Schwinnig, S., Small, E.A., Williams, D.G., 2004. Convergence across biomes to a common rain-use efficiency. *Nature* 429, 651–654.
- Jia, B., Tian, X., Xie, Z., Liu, J., Shi, C., 2013a. Assimilation of microwave brightness temperature in a land data assimilation system with multi-observation operators. *J. Geophys. Res.*, 118, <http://dx.doi.org/10.1002/jgrd.50377>.
- Jia, B., Xie, Z., Dai, A., Shi, C., Chen, F., 2013b. Evaluation of satellite and reanalysis products of downward surface solar radiation over East Asia: spatial and seasonal variations. *J. Geophys. Res.*, 118, <http://dx.doi.org/10.1002/jgrd.50353>.
- Jung, M., Reichstein, M., Bondeau, A., 2009. Towards global empirical upscaling of FLUXNET eddy covariance observations: validation of a model tree ensemble approach using a biosphere model. *Biogeosciences* 6, 2001–2013, <http://dx.doi.org/10.5194/bg-6-2001-2009>.
- Jung, M., Reichstein, M., Margolis, H.A., Cescatti, A., Richardson, A.D., Arain, M.A., Arneth, A., Bernhofer, C., Bonal, D., Chen, J., Gianelle, D., Gobron, N., Kiely, G., Kutsch, W., Lasslop, G., Law, B.E., Lindroth, A., Merbold, L., Montagnati, L., Moors, E.J., Papale, D., Sottocornola, M., Vaccari, F., Williams, C., 2011. Global patterns of land-atmosphere fluxes of carbon dioxide, latent heat, and sensible heat derived from eddy covariance, satellite, and meteorological observations. *J. Geophys. Res.* 116, G00J07, <http://dx.doi.org/10.1029/2010JG001566>.
- Katz, R.W., Glantz, M.H., 1986. Anatomy of a rainfall index. *Mon. Weather Rev.* 114, 764–771.
- Koven, C.D., Riley, W.J., Subin, Z.M., Tang, J.Y., Torn, M.S., Collins, W.D., Bonan, G.B., Lawrence, D.M., Swenson, S.C., 2013. The effect of vertically resolved soil biogeochemistry and alternate soil C and N models on C dynamics of CLM4. *Biogeosciences* 10, 7109–7131, <http://dx.doi.org/10.5194/bg-10-7109-2013>.
- Langley, J.A., Megonigal, J.P., 2010. Ecosystem response to elevated CO₂ levels limited by nitrogen-induced plant species shift. *Nature* 466, 96–99.
- Le Quéré, C., Raupach, M.R., Canadell, J.G., Marland, G., Bopp, L., Ciais, P., Conway, T.J., Doney, S.C., Feely, R.A., Foster, P., Friedlingstein, P., Gurney, K., Houghton, R.A., House, J.I., Huntingford, C., Levy, P.E., Lomas, M.R., Majkut, J., Metzl, N., Ometto, J.P., Peters, G.P., Prentice, I.C., Randerson, J.T., Running, S.W., Sarmiento, J.L., Schuster, U., Sitch, S., Takahashi, T., Viovy, N., van der Werf, G.R., Woodward, F.I., 2009. Trends in the sources and sinks of carbon dioxide. *Nat. Geosci.* 2, 831–836, <http://dx.doi.org/10.1038/ngeo689>.
- Lee, E., Felzer, B.S., Kothavala, Z., 2013. Effects of nitrogen limitation on hydrological processes in CLM4-CN. *J. Adv. Model. Earth Syst.* 5, 741–754, <http://dx.doi.org/10.1002/jame.20046>.
- Levis, S., Bonan, G., Vertenstein, M., Oleson, K., 2004. The Community Land Model's Dynamic Global Vegetation Model (CLM-DGVM): Technical Description and User's Guide, NCAR Technical Note NCAR/TN-459+STR. National Center for Atmospheric Research, Boulder, Colorado, pp. 50.
- Li, F., Levis, S., Ward, D.S., 2013. Quantifying the role of fire in the Earth system—Part 1: Improved global fire modeling in the Community Earth System Model (CESM1). *Biogeosciences* 10, 2293–2314, <http://dx.doi.org/10.5194/bg-10-2293-2013>.
- Liu, Y., Zhou, Y., Ju, W., Wang, S., Wu, X., He, M., Zhu, G., 2014. Impacts of droughts on carbon sequestration by China's terrestrial ecosystems from 2000 to 2011. *Biogeosciences* 11, 2583–2599, <http://dx.doi.org/10.5194/bg-11-2583-2014>.
- Lloyd Hughes, B., Saunders, M.A., 2002. A drought climatology for Europe. *Int. J. Climatol.* 22, 1571–1592, <http://dx.doi.org/10.1002/joc.846>.
- Lotsch, A., Friedl, M.A., Anderson, B.T., Tucker, C.J., 2005. Response of terrestrial ecosystems to recent Northern Hemispheric drought. *Geophys. Res. Lett.* 32, L06705, <http://dx.doi.org/10.1029/2004gl022043>.
- Mao, J., Thornton, P.E., Shi, X., Zhao, M., Post, W.M., 2012. Remote sensing evaluation of CLM4 GPP for the period 2000–2009. *J. Climate* 25, 5327–5342.
- McKee, T.B., Doesken, N.J., Kleist, J., 1993. The relationship of drought frequency and duration to time scales. 8th Conference on Applied Climatology, 179–184.
- McMurtrie, R.E., Norby, R.J., Medlyn, B.E., Dewar, R.C., Pepper, D.A., Reich, P.B., Barton, C.V.M., 2008. Why is plant-growth response to elevated CO₂ amplified when water is limiting but reduced when nitrogen is limiting? A growth-optimisation hypothesis. *Funct. Plant Biol.* 35, 521–534.
- Nemani, R.R., Keeling, C.D., Hashimoto, H., Jolly, W.M., Piper, S.C., Tucker, C.J., Myneni, R.B., Running, S.W., 2003. Climate-driven increases in global terrestrial net primary production from 1982 to 1999. *Science* 300, 1560–1563.
- Oleson, K.W., Lawrence, D.M., Bonan, G.B., Drewniak, B., Huang, M.Y., Koven, C.C., Levis, S., Li, F., Riley, W.J., Subin, Z.M., Swenson, S.C., Thornton, P.E., Bozbayik, A., Fisher, R., Heald, C.L., Kluzek, E., Lamarque, J., Lawrence, P.J., Leung, L.R., Lipscomb, W., Muszala, S., Ricciuto, D.M., Sacks, W., Sun, Y., Tang, J., Yang, Z.L., 2013. Technical Description of Version 4.5 of the Community Land Model (CLM). NCAR Technical Note NCAR/TN-503+STR. National Center for Atmospheric Research, Boulder, CO.
- Palmer, W.C., 1965. Meteorological Drought. Res. Dept. of Commerce, Washington, D.C. pp. 58 (Paper No.45).
- Pan, Y., Birdsey, R.A., Fang, J., Houghton, R., Kauppi, P.E., Kurz, W.A., Phillips, O.L., Shvidenko, A., Lewis, S.L., Canadell, J.G., Ciais, P., Jackson, R.B., Pacala, S.W., McGuire, A.D., Piao, S., Rautiainen, A., Sitch, S., Hayes, D., 2011. A large and persistent carbon sink in the world's forests. *Science* 333, 988–993, <http://dx.doi.org/10.1126/science.1201609>.
- Pei, F., Li, X., Liu, X., Lao, C., 2013. Assessing the impacts of droughts on net primary productivity in China. *J. Environ. Manage.* 114, 362–371.
- Piao, S.L., Fang, J.Y., Ciais, P., Peylin, P., Huang, Y., Sitch, S., Wang, T., 2009. The carbon balance of terrestrial ecosystems in China. *Nature* 458, 1009–1013.
- Piao, S.L., Ito, A., Li, S.G., Huang, Y., Ciais, P., Wang, X.H., Peng, S.S., Nan, H.J., Zhao, C., Ahlström, A., Andres, R.J., Chevallier, F., Fang, J.Y., Hartmann, J., Huntingford, C., Jeong, S., Levis, S., Levy, P.E., Li, J.S., Lomas, M.R., Mao, J.F., Mayorga, E., Mohammadi, A., Muraoka, H., Peng, C.H., Peylin, P., Poulet, B., Shen, Z.H., Shi, X., Sitch, S., Tao, S., Tian, H.Q., Wu, X.P., Xu, M., Yu, G.R., Viovy, N., Zaehle, S., Zeng, N., Zhu, B., 2012. The carbon budget of terrestrial ecosystems in East Asia over the last two decades. *Biogeosciences* 9, 3571–3586.
- Qian, W.H., Shan, X.L., Zhu, Y.F., 2011. Ranking regional drought events in China for 1960–2009. *Adv. Atmos. Sci.* 28 (2), 310–321, <http://dx.doi.org/10.1007/s00376-009-9239-4>.
- Reichstein, M., Bahn, M., Ciais, P., Frank, D., Mahecha, M.D., Seneviratne, S.I., Zscheischler, J., Beer, C., Buchmann, N., Frank, D.C., Papale, D., Rammig, A., Smith, P., Thoncik, K., van der Velde, M., Vicca, S., Walz, A., Wattenbach, M., 2013. Climate extremes and the carbon cycle. *Nature* 500, 287–295, <http://dx.doi.org/10.1038/nature12350>.
- Schwalm, C.R., Williams, C.A., Schaefer, K., Arneth, A., Bonal, D., Buchmann, N., Chen, J., Law, B.E., Lindroth, A., Luysaert, S., Reichstein, M., Richardson, A.D., 2010. Assimilation exceeds respiration sensitivity to drought: a FLUXNET synthesis. *Glob. Change Biol.* 16, 657–670.
- Shi, X., Mao, J., Thornton, P.E., Huang, M., 2013. Spatiotemporal patterns of evapotranspiration in response to multiple environmental factors simulated by the Community Land Model. *Environ. Res. Lett.* 8 (2), 024012, <http://dx.doi.org/10.1088/1748-9326/8/2/024012>.
- Stocker, T.F., Qin, D., Plattner, G.K., Tignor, M., Allen, S.K., Boschung, J., Nauels, A., Xia, Y., Bex, V., Midgley, P.M., 2013. *IPCC, 2013: Climate Change 2013: the Physical Science Basis. Working Group I Contribution to the Fifth Assessment Report of the Intergovernmental Panel on Climate Change*. Cambridge University Press Cambridge, UK and New York, NY, USA.
- Sun, X., Wen, X., Yu, G., Liu, Y., Liu, Q., 2006. Seasonal drought effects on carbon sequestration of a mid-subtropical planted forest of southeastern China. *Sci. China Earth Sci.* 49 (Suppl. II), 110–118.
- Thornton, P.E., Rosenbloom, N.A., 2005. Ecosystem model spin-up: estimating steady state conditions in a coupled terrestrial carbon and nitrogen cycle model. *Ecol. Model.* 189, 25–48.
- Thornton, P.E., Zimmermann, N.E., 2007. An improved canopy integration scheme for a land surface model with prognostic canopy structure. *J. Climate* 20, 3902–3923.
- Thornton, P.E., Lamarque, J.F., Rosenbloom, N.A., Mahowald, N.M., 2007. Influence of carbo-nitrogen cycle coupling on land model response to CO₂ fertilization and climate variability. *Glob. Biogeochem. Cycles* 21, B4018, <http://dx.doi.org/10.1029/2006GB002868>.
- Thornton, P.E., Doney, S.C., Lindsay, K., Moore, J.K., Mahowald, N., Randerson, J.T., Fung, I., Lamarque, J.F., Fedde, J.J., Lee, Y.H., 2009. Carbon-nitrogen interactions regulate climate-carbon cycle feedbacks: results from an atmosphere-ocean general circulation model. *Biogeosciences* 6, 2099–2120.
- Vicente-Serrano, S.M., Beguería, S., López-Moreno, J.I., 2010. A multi-scalar drought index sensitive to global warming: the Standardized Precipitation Evapotranspiration Index. *J. Climate* 23, 1696–1718.
- Viovy, N., 2011. CRUNCEP Dataset (Description Available at: <http://dods.extra.cea.fr/data/p529iov/cruncep/readme.htm>. Data available at <http://dods.extra.cea.fr/store/p529iov/cruncep/V4.1901.2012/>).
- Wang, L., Chen, W., 2014. A CMIP5 multimodel projection of future temperature, precipitation, and climatological drought in China. *Int. J. Climatol.* 29, 2059–2078, <http://dx.doi.org/10.1002/joc.3822>.
- Wang, Y., Xie, Z., Jia, B., Yu, Y., 2015. Simulation and evaluation of gross primary productivity in China by using land surface model CLM4. *Clim. Environ. Res. (in Chinese)* 20 (1), 97–110.

- Wu, C., Chen, J.M., 2013. Diverse responses of vegetation production to interannual summer drought in North America. *Int. J. Appl. Earth Observat. Geoinf.* 21, 1–6.
- Xiao, J.F., Zhuang, Q.L., Liang, E.Y., McGuire, A.D., Moody, A., Kicklighter, D.W., Shao, X.M., Melillo, J.M., 2009. Twentieth century droughts and their impacts on terrestrial carbon cycling in China. *Earth Interact.* 13 (10), 1–10, <http://dx.doi.org/10.1175/2009ei275.1>.
- Xie, Z., Wang, L., Jia, B., Yuan, X., 2016. Measuring and modeling the impact of a severe drought on terrestrial ecosystem CO₂ and water fluxes in a subtropical forest. *J. Geophys. Res. Biogeosci.* 121, <http://dx.doi.org/10.1002/2016JG003437>.
- Yuan, W., Liu, D., Dong, W., Liu, S., Zhou, G., Yu, G., Zhao, T., Feng, J., Ma, Z., Chen, J., Chen, Y., Chen, S., Han, S., Huang, J., Li, L., Liu, H., Liu, S., Ma, M., Wang, Y., Xia, J., Xu, W., Zhang, Q., Zhao, X., Zhao, L., 2014. Multiyear precipitation reduction strongly decrease carbon uptake over northern China. *J. Geophys. Res. Biogeosci.* 119, 881–896.
- Yuan, W., Cai, W., Chen, Y., Liu, S., Dong, W., Zhang, H., Yu, G., Chen, Z., He, H., Guo, W., Liu, D., Xiang, W., Xie, Z., Zhao, Z., Zhou, G., 2016. Severe summer heatwave and drought strongly reduced carbon uptake in Southern China. *Sci. Rep.* 6 (18813), <http://dx.doi.org/10.1038/srep18813>.
- Zeng, N., Qian, H., Roedenbeck, C., Heimann, M., 2005. Impact of 1998–2002 midlatitude drought and warming on terrestrial ecosystem and the global carbon cycle. *Geophys. Res. Lett.* 32, L22709, <http://dx.doi.org/10.1029/2005GL024607>.
- Zeng, X., Zeng, X., Barlage, M., 2008. Growing temperate shrubs over arid and semiarid regions in the Community Land Model-Dynamic Global Vegetation Model. *Global Biogeochem. Cycles* 22, GB3003, <http://dx.doi.org/10.1029/2007GB003014>.
- Zhang, L., Xiao, J., Li, J., Wang, K., Lei, L., Guo, H., 2012. The 2010 spring drought reduced primary productivity in southwestern China. *Environ. Res. Lett.* 6, 045706, <http://dx.doi.org/10.1088/1748-9326/6/4/045508>.
- Zhao, M.S., Running, S.W., 2010. Drought-induced reduction in global terrestrial net primary production from 2000 through 2009. *Science* 329, 940–943, <http://dx.doi.org/10.1126/science.1192666>.
- Zou, X.K., Zhai, P.M., Zhang, Q., 2005. Variations in droughts over China: 1951–2003. *Geophys. Res. Lett.* 32, L04707, <http://dx.doi.org/10.1029/2004GL021853>.
- Zscheischler, J., Reichstein, M., Harmeling, S., Rammig, A., Tomelleri, E., Mahecha, M.D., 2014. Extreme events in gross primary production: a characterization across continents. *Biogeosciences* 11, 2909–2924, <http://dx.doi.org/10.5194/bg-11-2909-2014>.